3-10-2010

In-situ, Gate Bias Dependent Study of Neutron Irradiation Effects on AlGaN/GaN HFETs

Janusz K. Mikina

IN-SITU GATE BIAS DEPENDENT STUDY OF NEUTRON IRRADIATION EFFECTS ON ALGAN/GAN HFETS

THESIS

Janusz K. Mikina, Captain, USAF

AFIT/GNE/ENP/10M-06

DEPARTMENT OF THE AIR FORCE
AIR UNIVERSITY

AIR FORCE INSTITUTE OF TECHNOLOGY

Wright-Patterson Air Force Base, Ohio

The views expressed in this thesis are those of the author and do not reflect the official policy or position of the United States Air Force, Department of Defense, or the U.S. Government.

AFIT/GNE/ENP/10M-06

IN-SITU GATE BIAS DEPENDENT STUDY OF NEUTRON IRRADIATION EFFECTS ON ALGAN/GAN HFETS

THESIS

Presented to the Faculty

Department of Engineering Physics

Graduate School of Engineering and Management

Air Force Institute of Technology

Air University

Air Education and Training Command

In Partial Fulfillment of the Requirements for the

Degree of Master of Science in Nuclear Engineering

Janusz K. Mikina, BS

Captain, USAF

March 2010

AFIT/GNE/ENP/10M-06

IN-SITU GATE BIAS DEPENDENT STUDY OF NEUTRON IRRADIATION EFFECTS ON ALGAN/GAN HFETS

Janusz K. Mikina, BS
Captain, USAF

Approved:

_____	_____
Lt Col John W.McClory (Chairman)	Date
_____	_____
James C. Petrosky, PhD (Member)	Date
_____	_____
Robert L. Hengehold, PhD (Member)	Date

AFIT/GNE/ENP/10M-06

Abstract

AlGaN/GaN Heterostructure Field Effect Transistors (HFETs) have come under increased study in recent years due to their highly desirable material and electrical properties and survivability even during and after exposure to extreme temperature and radiation environments. In this study, unpassivated and SiN passivated $Al_{0.27}Ga_{0.73}N$/GaN HFETs were subjected to neutron radiation at 120 K. The primary focus of the research was the effects of neutron irradiation on drain current, gate leakage current, threshold voltage shift, gate-channel capacitance, and the effects of biasing the gate during irradiation. In-situ measurements were conducted on transistor current, gate-channel capacitance, and gate leakage current vs. gate bias beginning at 77 K through 300 K in 4 K temperature intervals. The drain currents increased for all devices, with a lesser increase observed for passivated devices. The changes in carrier concentration and carrier mobility, obtained from observed drain current increases and calculated with the charge control model using observed threshold voltage shifts, were attributed to trapped, positive charges in the AlGaN layer. This trapped positive charge resulted from electron-hole pairs created by neutron radiation-induced ionizations. The leakage current increased in all devices, with a smaller change observed in passivated devices. This increase was attributed to the formation of interface traps. Biasing the gate under neutron irradiation had no effect on the electrical performance of HFETs.

Acknowledgments

I want to thank the members of my board, Dr. Robert Hengehold, Dr. James Petrosky and Lt Col John McClory, for their patience, time and effort teaching and advising me during my research. Lt Col McClory special thanks to you for your constructive criticism, my AFIT experience would have been much harder without you. Dr. Bridgeman, Dr. Burggraf and Dr. Mathews, I was very lucky to have such experienced teachers with unique expertise, I felt honored to be your student. Dr. Benjamin Kowash, your knowledge at such a young age is hard to find. AFIT is lucky to have you as an instructor. To the crew in the AFIT workshop, thank you for making my test possible. Your manufacturing and design expertise is second to none. Eric Taylor, thank you for everything you've done for me, ordering equipment, and taking care of software and equipment issues.

And, last but not least, I want to thank my family for their support.

Janusz K. Mikina

Table of Contents

Page

List of Figures

Page

Page

List of Tables

Table Page

List of Symbols

C_{gs}	Gate Capacitance
E	Electric Field
g_d	Drain Conductance
g_m	Transconductance
I_{ds}	Drain-Source Current
I_{dsat}	Saturation Drain-Source Current
I_{gs}	Gate-Source Current
$I_{leakage}$	Leakage Current
V_{ds}	Drain-Source Voltage
V_{gs}	Gate-Source Voltage
V_{th}	Threshold Voltage
q	Charge
μ	Carrier Mobility

List of Abbreviations

2DEG	Two Dimensional Electron Gas
AlN	Aluminum Nitride
AlGaN	Aluminum Gallium Nitride
DT	Direct Tunneling
FET	Field Effect Transistor
GaN	Gallium Nitride
GaAs	Gallium Arsenide
HEMT	High Electron Mobility Transistor
HFET	Heterojunction Field Effect Transistor
MODFET	Modulation Doped Field Effect Transistor
MOVPE	Metal-Organic Vapor-Phase Epitaxy
PECVD	Plasma Enhanced Chemical Vapor Deposition
Si	Silicon
SiN	Silicon Nitride
SiC	Silicon Carbide
SMU	Source-Measure Unit
TAT	Trap Assisted Tunneling
TC	Thermocouple

IN-SITU GATE BIAS DEPENDENT STUDY OF NEUTRON IRRADIATION EFFECTS ON ALGAN/GAN HFETS

I. Introduction

1. Background

The application of different semiconductor structures in electronic components is extensive and continues to grow. Heterojunction aluminum gallium nitride (AlGaN) and gallium nitride (GaN) structures have been developed over the past decade for a number of specific applications. The increased carrier mobility, higher power density, and better radiation hardness than silicon and gallium arsenide based structures make them a very attractive alternative to silicon (Si) and gallium arsenide (GaAs) based semiconductors. Due to the wide band gap and high breakdown field, AlGaN devices can operate at very high temperature and operating frequency. AlGaN/GaN based structures, have been used as inverters, relay switching devices, and high-temperature sensors. Their inherent radiation hardness as compared to silicon and gallium arsenide devices makes them a natural choice for military applications in harsh radiation, space and nuclear environments [1][2]. Military applications range from aircraft and rocket controllers, missile plume detectors, submarine communication systems, to wireless communications and phased array radar systems.

The focus of this study is on the neutron environment effects. The neutron environment can be very damaging to semiconductors. Therefore any increase to radiation hardness is of great importance for applications in high neutron flux environments.

2. Research Focus

The research focuses on radiation effects in $Al_{0.27}Ga_{0.73}N/GaN$ heterojunction field effect transistors. In particular, the following questions will be addressed.

1) Can irradiation effects be mitigated by biasing the gate during irradiation?

2) Are there any additional transient effects not observed to date, that contribute to the degradation of HFETs performance under radiation? Can they be qualitatively and quantitatively analyzed?

3) At what rate do interface traps form and how is this rate dependent on the radiation type?

4) Is charge created through radiation interactions? If so, where is it created, is it mobile and what effect does it have on the device electrical characteristics?

5) What is the nature of the interface traps and where are they created?

II. Theory

1. GaN and AlN Crystals

The GaN crystals can be either have a wurtzite or zinc-blend structure, depending on the growth technique. Most GaN semiconductors used in electronic component applications have a wurtzite structure because it is thermodynamically stable under ambient conditions [3]. GaN has a wide, direct band gap of 3.4 eV. It is therefore suitable for high temperature devices. Its high breakdown field and high carrier mobility field make it ideal for use in high power and high frequency devices.

The Aluminum Nitride (AlN) like GaN can also be grown with a wurtzite crystal structure and has a band-gap of 6.1 eV. Aluminum, due to having smaller atoms than gallium, forms a smaller crystal cell with nitrogen than the gallium, resulting in a smaller lattice constant. Since aluminum is very reactive and has large affinity to oxygen, the contamination of AlN with oxygen is unavoidable.

2. Al_xGaN_{1-x}/GaN Heterojunction Structures

a) Spontaneous and Piezoelectric Polarization

Due to the fact that AlN can form alloys with GaN, it is suitable for creation of the AlGaN/GaN structures described here. The band-gap of AlGaN alloys depends on the molar fraction of aluminum and for 27% aluminum molar fraction the band gap is 0.42 eV [4].

An unstrained AlGaN/GaN crystal has a built-in polarization field referred to as spontaneous polarization. This polarization is a result of lack of symmetry in the GaN crystal. The lack of symmetry causes the electron charge cloud to shift resulting in

positive charge on one end of the crystal and negative on the on the other end. The piezoelectric polarization is a result of mismatch in lattice constants between the GaN and AlGaN crystals. Along the Ga-face, the piezoelectric polarization field points in the same direction as the field induced by spontaneous polarization, i.e. towards the substrate.

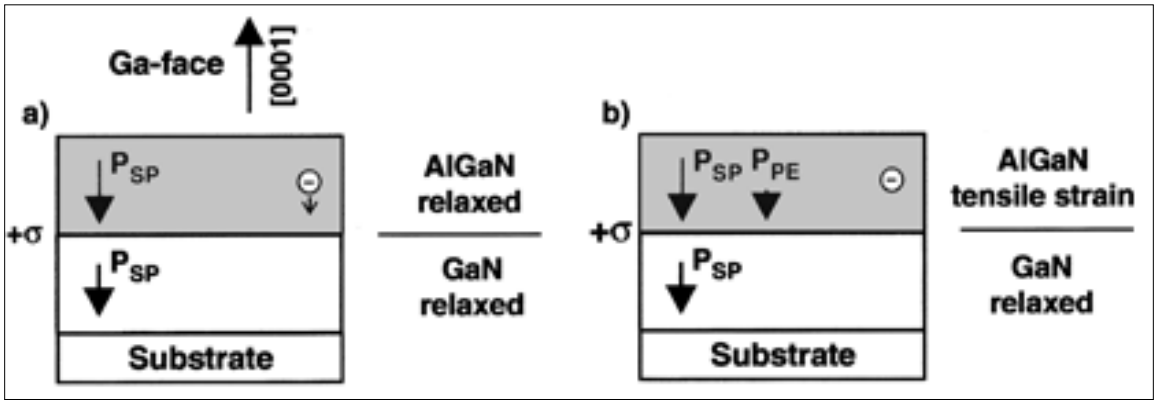

Figure 1. Spontaneous and piezoelectric polarization in the Ga-face AlGaN/GaN structure and polarization resulting from unstrained and strained crystals. (Reproduced without permission from O. Ambacher, Journals of Applied Physics, 15 March 1999)

Equations approximating total polarization are presented by Ambacher [5] and shown in (1)-(3) for the AlGaN/GaN interface, where x is the aluminum fraction of the semiconductor, P_{sp} is the spontaneous polarization (2), and the P_{pe} is the piezoelectric polarization given by (3).

$$P_{AlGaN/GaN}(x) = P_{sp}(x) + P_{pe}(x) - P_{sp}(0) \quad (1)$$

$$P_{sp}(x) = (-0.052\,x - 0.029)\ [C/m^2] \quad (2)$$

$$P_{pe}(x) = \frac{(-17.1025\,x - 6.73188\,x^2 - 0.008125\,x^3)}{(524.166 - 54.0718\,x + x^2)} \quad [C/m^2] \tag{3}$$

b) 2-Dimensional Electron Gas Formation (2DEG)

The polarization induced sheet charge density, $\sigma(x)$, can be approximated by [5]

$$\sigma(x) = P_{sp}(AlGaN) + P_{pe}(AlGaN) - P_{sp}(GaN) - P_{pe}(GaN) \tag{4}$$

The 2 DEG is formed when free electrons compensate the positive charges induced by polarization. A band diagram of the AlGaN/GaN heterojunction along with the 2-dimensional electron gas (2 DEG) is shown in Figure 2. The 2 DEG has a nominal width of a few nanometers and typical densities on the order of 10^{13} electrons/cm^2.

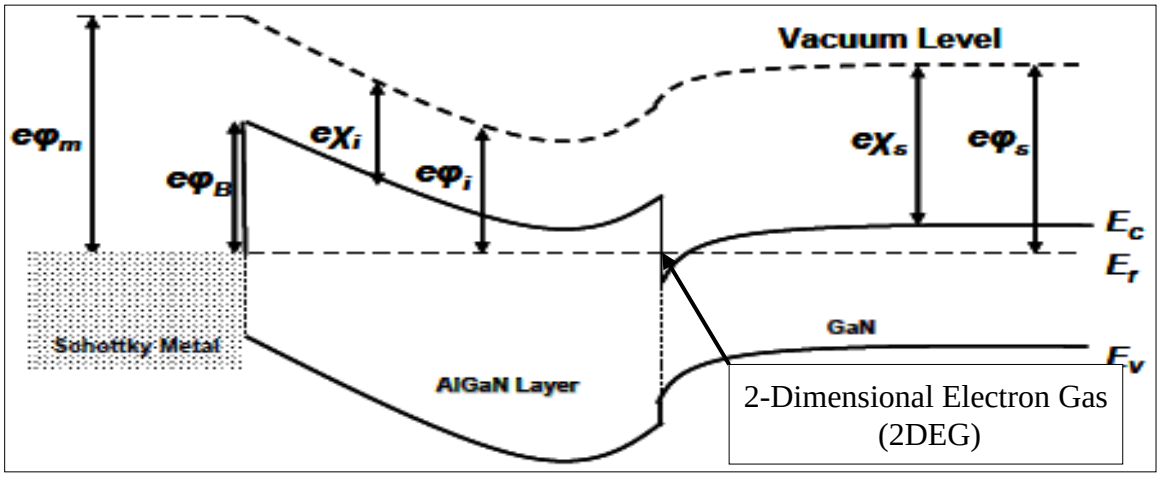

Figure 2. Schottky metal, AlGaN and GaN band diagram. Schottky barrier is created when metal is in contact with a semiconductor. The heterojunction is formed at the AlGaN/GaN boundary. 2 DEG forms, giving HFETs its high carrier mobility properties. Figure was reproduced without permission [15]

The sheet charge, $n_s(x)$, concentration is given by [6],

$$n_s(x) = \frac{\varepsilon(x)}{q\,d}\left(V_{gs} - V_{th}(x) - \frac{E_f}{q}\right) \tag{5}$$

where, $\varepsilon(x)$ is the dielectric constant depending on the molar fraction of aluminum, d is the thickness of the AlGaN layer, V_{gs} is the gate voltage, E_f is the Fermi energy and $V_{th}(x)$ is the molar fraction dependent threshold voltage given by

$$V_{th}(x) = \phi_b(x) - \Delta\phi_c(x) - \frac{q\,N_d\,d^2}{2\,\varepsilon(x)} - \frac{\sigma(x)}{\varepsilon(x)} \tag{6}$$

Here, ϕ_b is the Schottky barrier height, $\Delta\phi_c$ is the change in conduction band voltage and N_d is the donor density of the AlGaN layer. The Schottky barrier height, ϕ_b, in AlGaN can be approximated using equation (7), ref. [5] or equation (8) ref. [7]

$$e\phi_b = (1.3\,x + 0.84)\ [eV] \tag{7}$$

$$e\phi_b = (1.8559\,x + 0.7841)\ [eV] \tag{8}$$

where, x is the molar fraction of aluminum, in this case 0.27, giving the Schottky barrier height of 1.19 eV or 1.28 eV, respectively.

In GaN the bulk mobility peaks around 180 K. At temperatures lower than 180 K, the bulk mobility is limited by impurity scattering and decreases as temperature decreases. Above 180 K the mobility decreases due to the increase in phonon scattering. In HFETs, the 2 DEG layer provides a channel for the free carriers to flow (Figure 3). Due to its small cross section, a few nanometers, the effects of impurity scattering are minimized and the mobility inside the 2 DEG channel does not decrease below 80 K as the bulk mobility does [10].

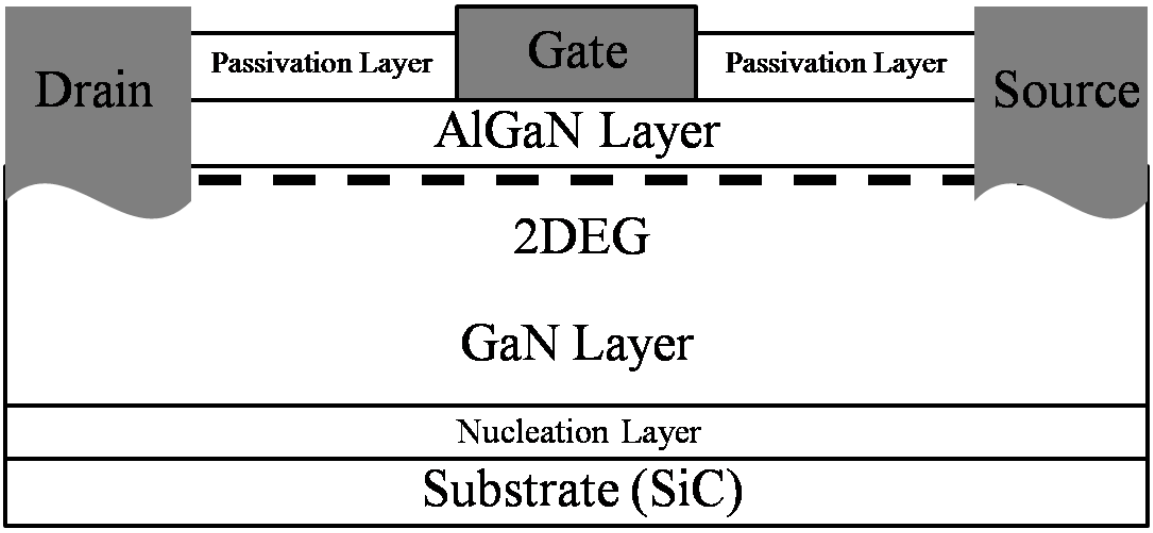

Figure 3. HFET's cross section showing formation of 2 DEG [8] at the AlGaN/GaN interface.

In addition to phonon scattering, interface traps can also decrease the mobility by providing scattering sites. Electrons trapped by these interface traps do not contribute to I_{ds}, or drain conductance, but can affect capacitance and threshold voltage. The field effective mobility of carriers can be estimated by measuring the drain conductance of a device and is approximated by

$$\mu_{eff} = \frac{g_d \; L}{W \, C_g \; (V_{gs} - V_{th})} \tag{9}$$

where W is the gate width, L is the gate length, C_g is the gate capacitance per unit area, V_{gs} is the gate-source voltage, V_{th} is the threshold voltage and the drain conductance, g_d is expressed as

$$g_d = \left. \frac{\partial I_{ds}}{\partial V_{ds}} \right|_{V_{gs}} \tag{10}$$

while, the transconductance, g_m, is defined as the change in current I_{ds} divided by change in gate-source voltage $V_{gs,}$ or can be calculated using equation (12).

$$g_m = \left.\frac{\partial I_{ds}}{\partial V_{gs}}\right|_{V_{ds}} \tag{11}$$

$$g_m = \frac{W}{L}\mu_{EF} C_g V_{ds} \tag{12}$$

3. Trap-Assisted Tunneling Model (TAT)

The trap-assisted tunneling model describes how electrons can tunnel from the gate metal through the Schottky barrier to the traps inside the AlGaN layer. The model then describes how the electrons continue to tunnel through the low AlGaN/GaN barrier into the channel where they are swept up by applied bias into the drain or source. This model was developed and refined by Karmalkar and Sathaiya [11][12]. This model shows that the trap-assisted tunneling dominates at temperature below 500 K and direct tunneling (thermionic field emission) dominates at higher temperatures. The gate current consists of two processes, the trap-assisted tunneling, I_{TAT}, and direct tunneling, I_{DT}.

$$I_G = I_{TAT} + I_{DT} \tag{13}$$

The trap-assisted tunneling component I_{TAT} is expressed by

$$I_{TAT} = \frac{q\,A}{E}\int_{\phi_T}^{\phi_b + V_g} R d\phi \tag{14}$$

.

Here, the q is the elemental charge, A is the gate area, E is the electric field, Φ_b is the Schottky barrier, Φ_T is the traps energy and V_g is the gate voltage and the tunneling rate R can be approximated using equation (15).

$$\frac{1}{R} = \frac{1}{R_1} + \frac{1}{R_2} \tag{15}$$

R_1 is the rate of tunneling through the Schottky barrier into a trap and R_2 is the rate of tunneling from the trap into the AlGaN layer. The rate R_1 and R_2 are given by,

$$R_1 = C_t \, f_{FD} \, N_t \, P_1 \tag{16}$$

and

$$R_2 = C_t \, N_t \, P_2 . \tag{17}$$

Here, f_{FD} is the Fermi-Dirac occupancy fraction, P_1 is the probability of tunneling through the Schottky barrier into the trap, C_t is the rate constant, N_t is the trap density and P_2 is the probability of electron tunneling from the trap into the AlGaN layer. These are given by,

$$P_1 = e^{-\frac{\alpha}{E}\left(\phi^{\frac{3}{2}} - \phi_t^{\frac{3}{2}}\right)}, \; P_2 = e^{-\frac{\alpha}{E}\phi_t^{\frac{3}{2}}} \; and \; \alpha = \frac{8\,\pi\,\sqrt{2\,m\,q}}{3\,h} \tag{18}$$

$$C_t = \frac{16\,\pi\,q\,E_1^{\frac{3}{2}}}{3\,h\,\sqrt{\phi_b - E_1}} \tag{19}$$

where, the total average electron energy, E_1 = 0.2 V [13]. Combining equations (14) through (18) gives

$$I_{TAT} = \frac{q\,A\,C_t\,N_t}{E} \int_{\phi_T}^{\phi_b + V_g} \frac{1}{f_{FD}\,P_1} + \frac{1}{P_2} \, d\phi \tag{20}$$

4. Radiation Effects on AlGaN/GaN Structures

GaN crystal damage has been studied extensively and defects are well known. The HFETs used in this study are made of four types of materials: AlGaN, GaN, SiN and SiC. Understanding native (as-grown) defects as well as defects resulting from radiation damage is crucial to understanding their effects on HFET electrical characteristics.

The research in [14] by Hogsed, focused on identification of AlGaN defects after electron irradiation via DLTS and discovered a new trap site, R4, attributed to aluminum displacements. Hogsed showed that the levels of traps deepened as the mole fraction of aluminum increased. The two properties most affected by the radiation displacement damage will be the mobility and carrier concentration [15][16][17][18][19]. Charge defects resulting from displacement damage can affect the 2 DEG concentration. Inside the AlGaN layer, positively charged defects will increase the overall strength of the polarization field and in turn increase the electron concentration at the interface, affecting the transistor current and the threshold voltage. The opposite is true for negatively charged defects. Defects created inside the GaN layer have the opposite effect and can also affect the transistor current and the threshold voltage, V_{th}. The carrier mobility can be affected by the scattering sites created by atom displacement.

A change in carrier concentration can be calculated to quantitatively analyze the effects of neutron radiation. The drain current, I_{ds} is proportional to the charge q, gate width W, carrier's drift velocity, ν and charge concentration n_s as shown in (21). The velocity of carriers can be calculated using equation (22), where μ is the mobility of a carrier and E is the applied field. By measuring the changes in I_{ds} we can determine the

change in carrier concentration using equation (23). In addition to the drain current method, the change in carrier concentration can be calculated using the threshold voltage. Equation (24) from Rashmi [6] shows that the change in charge density can found by measuring the changes in the threshold voltage pre and post-irradiation. The ε is the dielectric constant, q is the charge, d is the thickness of the AlGaN layer and ΔV_{th} is the change in threshold voltage which in this experiment was measured using the linear extrapolation and transconductance techniques [10].

$$I_{ds} = - q W v n_s \tag{21}$$

$$v = \mu E \tag{22}$$

$$\Delta n_s = \frac{\Delta I_{ds}}{q W v} \tag{23}$$

$$\Delta n_s = \frac{\varepsilon}{qd} (-\Delta V_{th}) \tag{24}$$

5. Effects of Passivation on HFETs Performance

Passivated transistors in this study had a layer of silicon nitride (Si_3N_4) covering the AlGaN layer between the source, drain and gate. The transistors used in this study were passivated using the Plasma Enhanced Chemical Vapor Deposition (PECVD) method. The effects of passivation are not fully understood. The proposed mechanism for explaining this effect is the reduction in electron trapping at the surface [20][21]. In unpassivated devices trapped surface electrons counter the induced polarization field and as a result reduce the sheet charge density of the 2 DEG as depicted in Figure 4. The

passivation layer covers the exposed AlGaN layer and prevents electrons leaking from the gate metal from being trapped at the surface. In addition, the passivation layer minimizes the amount of negative state charges created by radiation [21]. Passivation has been reported [20] to increase the sheet charge density by 27%, and transistor saturation current by 37% over similar unpassivated devices.

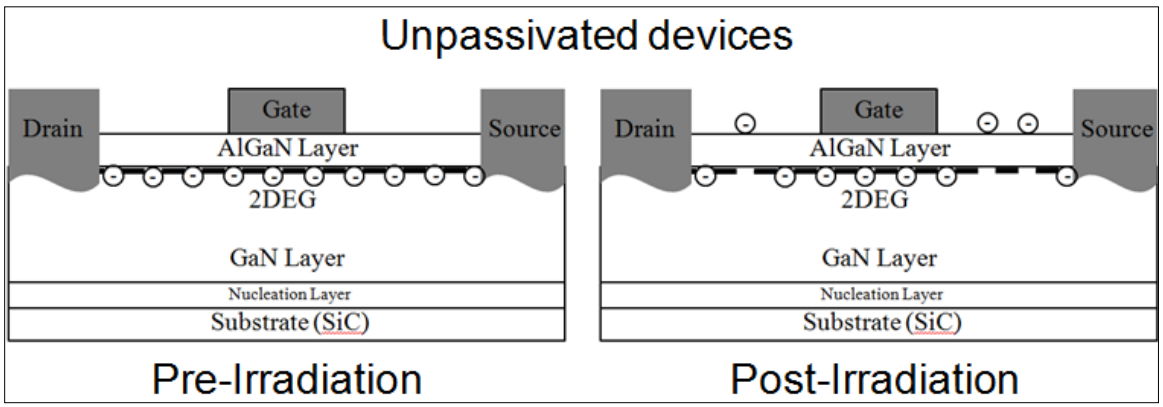

Figure 4. Pre and post irradiation depiction of 2DEG affected by negative surface charges created by radiation.

6. Neutron Damage

When discussing neutron damage it is useful to talk about the damage in terms of one neutron energy equivalent. The ASTM 722 standard was used to calculate the 1MeV equivalent neutron fluence in gallium arsenide. Gallium arsenide was chosen instead of Si due to more similar structure to GaN. The equivalent fluence, $\phi_{eq,Eref,mat}$ for a given material is given by

$$\phi_{eq,Eref,mat} = \frac{\int_0^{\infty} \phi(E) F_{D,mat}(E) dE}{F_{D,Eref,mat}} \tag{25}$$

where, $\phi(E)$ is the energy-fluence spectral distribution function, $F_{D,mat}(E)$ is the energy dependent fluence damage function for a specific material and $F_{D,Eref,mat}$ is the equivalent energy dependent displacement damage value of a reference material. For gallium arsenide this value is 70 MeV mbarn.

III. Previous Research

This chapter discusses results of various neutron and proton irradiation studies on AlGaN/GaN heterojunctions conducted in the past. To understand the effects of neutron radiation on AlGaN/GaN devices it is important to understand the damage mechanism caused not only by neutrons, but also protons. Although the non-ionizing energy loss can be different for neutrons and protons, both can cause displacement damage. Therefore understanding the effects of proton irradiation on AlGaN/GaN heterojunctions can be useful when discussing neutron damage.

1. Proton Irradiation

In 2002, White et al., [22] used the nanoscale depth-resolved luminescence spectroscopy method to study the degradation of transistor current after irradiating AlGaN/GaN MODFETs and an HFET transistor with 1.8 MeV protons. They observed a decrease in MODFET saturation current, drain current and transconductance and attributed these changes to the decrease in electric field within the AlGaN layer caused by charged defects.

Similarly, Gaudreau, et al. [23] studied effects of 2 MeV proton irradiated MODFETs. Resistivity and Hall effect measurements results showed that the carrier density was decreased by a factor of two and mobility degradation by a factor of a thousand when devices were exposed to proton fluences between $1x10^{13}$ and $7x10^{15}$ cm^{-2}. Gaudreau provided evidence that the carrier concentration dropped gradually with fluence, but the mobility had a tendency drop rapidly by relatively large values. He concluded that the device failure was mainly caused by the mobility degradation.

Hu, et al. [24] measured degradation of HEMTs after irradiating them with various energy protons ranging from 1.8 MeV up to 105 MeVs at fluences up to 10^{13} cm^{-2}. Transistors irradiated with the 15, 40 and 105 MeV protons recovered fully after annealing at room temperature. A fluence of 10^{12} cm^{-2} 1.8 MeV protons created lasting damage to transistors resulting in 10.6% saturation current decrease and a 6.1% decrease in transconductance.

2. Neutron Irradiation

Polyakov et al. [19] irradiated $Al_{0.3}Ga_{0.7}N$/GaN devices grown by MOCVD on sapphire at room temperature. He observed a decrease in the mobility and sheet conductivity after exposure to $10^{15}cm^{-2}$. The sheet concentration did not change greatly at RT (~10% after 10^{17} cm^{-2}), while the changes in mobility were ~20% after $4x10^{15}$ cm^{-2}. Electron traps were identified at with activation energies of 0.21, 0.35 and 0.45 eV in the AlGaN layer in addition to hole traps which had energies of 0.18, 0.2, 0.26, 0.7 and 1eV. The location of these hole traps was not identified, but suspected to be located inside either the AlGaN barrier or the GaN layer.

Similar results were observed in another study [18] by Polyakov a year earlier, when he irradiated n-doped AlGaN/GaN devices and saw a decrease in mobility at fluences above 10^{14} n/cm^{-2}. The sheet concentration did not significantly decrease until the fluence of $2.5x10^{16}$ n/cm^{2} was reached. In both studies the mobility decreased at fluences two orders of magnitude lower than the onset of significant sheet concentration degradation.

Extensive studies on neutron irradiated AlGaN/GaN structures have been ongoing at AFIT. Uhlman [25] conducted the first irradiation of AlGaN/GaN HFETs with 1MeV

equivalent neutrons. He observed an increase in gate leakage and drain currents at 77 K. These effects were not observed when irradiations were performed at temperatures above 300 K. Additionally, he demonstrated that tunneling across the Schottky gate occurs due to the effective lowering of the Schottky barrier by irradiation induced defects.

Gray [26] irradiated AlGaN/GaN structures with neutrons at fluences of $4.0x10^{10}$ and $1.2x10^{12}$ neutrons/cm^2. He confirmed an increase in gate leakage current with an increase in fluence and attributed it to an increase in deep trap formation that resulted in a trap assisted tunneling current. Also, a threshold voltage increase was recorded and attributed to increases in donor defect density.

McClory [15] studied the temperature dependent changes to drain and gate currents in HFETs under electron and neutron irradiation for both passivated and un-passivated devices. His studies showed susceptibility to threshold voltage shifts and changes to drain currents after irradiation, but the HFETs continued to operate as transistors after irradiation fluencies of up to 10^{14} 0.45 MeV equivalent electrons/cm^2 or 10^{13} 1 MeV equivalent neutrons/cm^2. The threshold voltage increased (became more negative) and drain currents increased after irradiation at 80 K. McClory observed that when the HFETs were warmed to 300 K after irradiation these effects annealed and the electrical parameters returned to their pre-irradiation values. The conclusion was that positive charges trapped in the AlGaN layer were responsible for the effect at low temperature. As the temperature increased, the additional kinetic energy of the trapped charge caused the charges to become mobile allowing them to migrate towards the interface under the

influence of the intrinsic electric field. It was suggested that at the surface the charges recombine or become charged defects.

The leakage current was increased after electron and neutron irradiation and persisted to 300 K. It occurred at relatively low doses and even after weeks of annealing the increase in current remained. McClory attributed it to the permanent defects in the AlGaN layer. He hypothesized that complexing of gallium, aluminum, and nitrogen defects with impurities was the cause for this behavior and suspected that oxygen ions were the key component of the defect complexing. McClory also confirmed that passivation provides radiation hardening by neutralizing the negative charges created by radiation. The changes in characteristics of the devices were smaller in passivated as compared to un-passivated HFETs.

Following McClory's research, Moran [16] studied the effects of electron irradiation and temperature on the threshold voltage, gate leakage current, and gate channel capacitance. Based on I_{ds}-V_{ds} and C_{gs}-V_{gs} measurements, Moran affirmed that the drain current increases post-irradiation and that most devices returned to nearly pre-irradiation levels after annealing at 300 K. The threshold voltage shifts and leakage currents resulting from irradiation also returned to pre-irradiation levels after 300 K annealing in unpassivated devices. The passivated devices' leakage current remained unchanged after annealing, a result of permanent damage to the passivation layer.

Uhlman suggested in-situ measurements as a means to extend this research area. He also suggested that the transport through Schottky contacts should be investigated. McClory recommended examining the passivation layer defects through the use

spectroscopic methods. Additionally, he proposed investigation of oxygen ion effects on electrical performance of HFETs. Finally, Moran proposed investigation of time dependent interface trap formation versus dose and irradiation (gamma vs. neutron) as well as in-situ transient effect with varying gate voltage.

3. Summary

As described in this chapter, the AlGaN/GaN structures have been studied extensively under different radiation types; however, there had been no completed in-situ studies of transient effects in HFETs. This research was focused on filling in that gap and addressing some of the issues and recommendations put forth by previous researchers. This was achieved by in-situ measurement of HFETs response to neutron radiation under varying gate biases.

IV. Experimental Procedures

This chapter contains a detailed description of the devices, equipment, and facilities used in the neutron irradiation experiments, in addition to the calibration and data acquisition procedures.

1. Ohio State University Research Reactor

The in-situ experiments were conducted at the Ohio State University Research Reactor (OSURR). The OSURR is a 500 kW light water pool-type reactor with multiple access ports. For the purpose of this study the 7" vertical irradiation tube was selected. This irradiation tube design and characteristics are described by Gray [26] and was located inside the reactor pool against the reactor core, as shown in Figure 12. Although Gray performed the spectrum and flux analysis inside the tube, a new analysis was required. This spectrum and flux analysis was necessary after the development of a new irradiation chamber described in the next paragraph.

2. Irradiation Chamber Design and Analysis

The neutron irradiation chamber used in this research was custom designed to minimize activation, cool the devices down to 77 K and allow measurement inside the 7" vertical irradiation tube [26]. To maximize the fluence on the devices the chamber was designed to place the HFETs 13" above the bottom of the irradiation tube based on the flux intensity show in Figure 5.

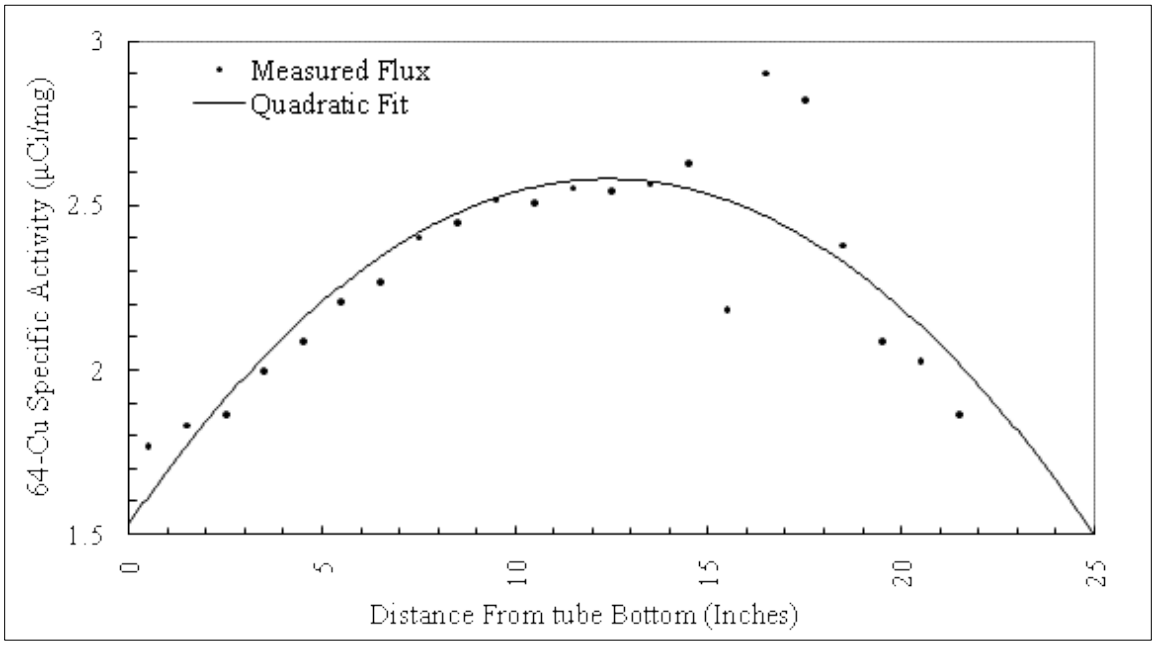

Figure 5. Activity of copper wires used for neutron flux measurements versus distance from the bottom of the irradiation tube. The optimal location for highest flux is at about 13" from the bottom.

Due to the radiation environment, reasonable care was taken to minimize neutron activation. The frame was made of Aluminum 6061 which was chosen because of a combination of aluminum's strength, short half-life of activated isotopes, weight and cost. Aluminum has a thermal neutron cross section of 0.23 barns and the activated isotope ^{128}Al has a half-life of 2.25 minutes, hence the activity decreases rapidly following neutron irradiation. This material also has a small percentage of impurities, thus minimizing activation.

The reactor radiation spectrum consists of neutrons of various energies, resulting from fission reactions, as well as primary and secondary gamma radiation. Primary gamma radiation is a result of fission, whereas secondary gamma radiation from neutron capture in hydrogen and other atoms. The spectrum can be manipulated using various materials.

A 1mm thick cadmium sheet was used to surround the devices to minimize activation by absorbing thermal neutrons and thereby "hardening" the spectrum. The cadmium absorption cross section is shown in Figure 6. The thermal neutron flux can be reduced by almost four orders of magnitude by using a 1 mm cadmium shield, therefore reducing activation by a large factor.

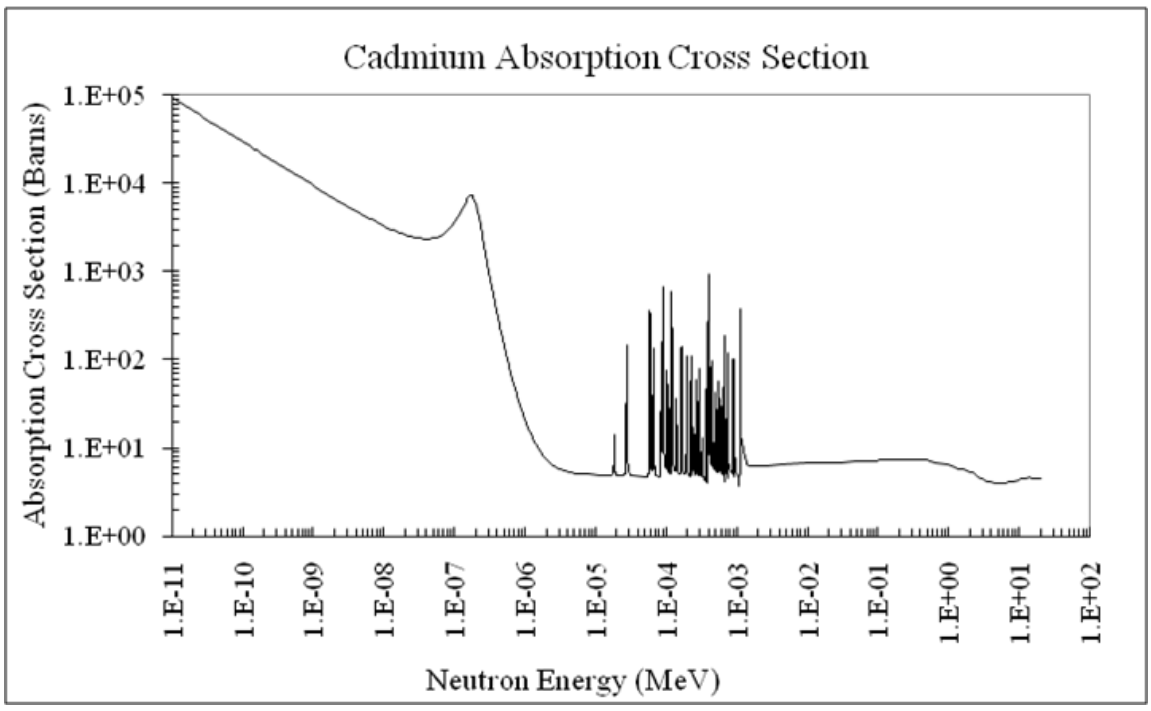

Figure 6. Cadmium absorption cross section. A reduction of almost four orders of magnitude in thermal neutrons can be achieved by using a 1 mm thick cadmium shield.

The reduction of gamma rays is most effective when using high Z materials, such as lead. The neutron shielding should be "in front" of the gamma ray shielding to reduce secondary gamma rays. The high energy gamma rays created inside of a reactor have a very low probability of interaction inside the semiconductor which has a thickness of less than 1 mm, and using large amounts of dense materials would also result in a neutron

flux drop. Gamma radiation has been shown to have little effect on electrical properties of passivated AlGaN/GaN HFETs until a dose of over 300 Mrad (Si) was reached [27]. Unpassivated devices have been shown to be affected by gamma radiation by Luo, et al. [28]. At a dose of 1 Mrad (Si) they observed a decrease in I_{ds} and transconductance while the threshold voltage was relatively unchanged. The gamma ray dose inside the OSURR 500 kW reactor where the irradiation tube was placed was estimated to be, ~15 Mrad (tissue) [29]. The irradiation chamber was design to accommodate 3 cm of shielding material.

The sample holder/cold finger (Figure 7) was constructed using one piece of aluminum to minimize activation and to allow devices to be cooled down to 77 K. Multiple devices can be mounted on the sample holder depending on the device size. In this study two devices were mounted side by side.

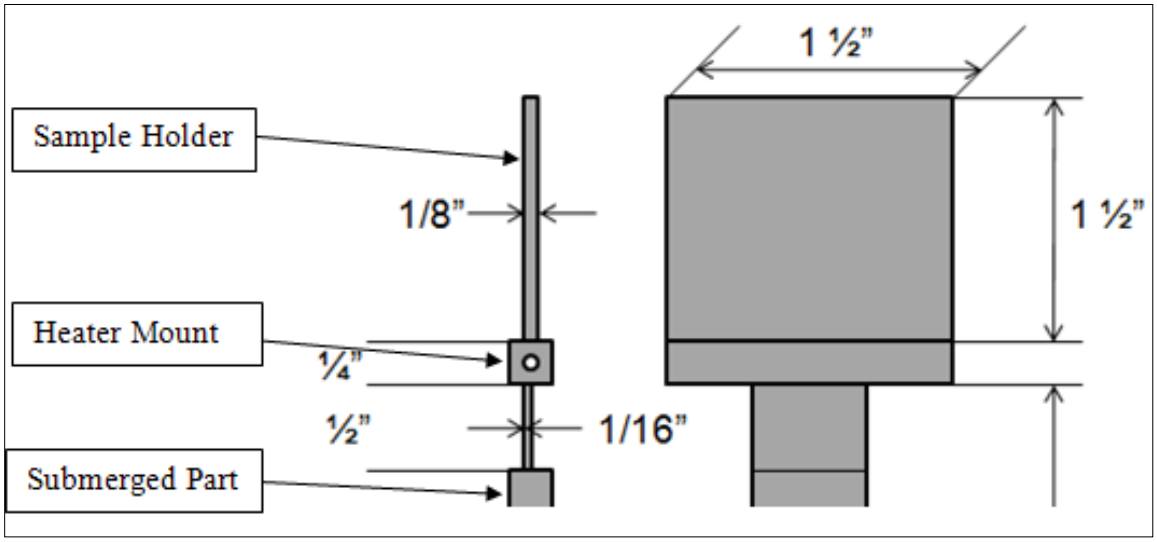

Figure 7. Cold finger with aluminum 6061 sample holder on which the devices were mounted. The TC was attached to the back surface at the same vertical distance as the center of HFETs

An opening for a heater was drilled at the bottom of the sample holder to provide the capability to heat up the samples without removing the cold finger assembly out of the Dewar if necessary. A neutron spectrum analysis was performed inside this irradiation chamber. A standard foil activation method was used. Gold, cobalt and copper wires were attached to a cold finger where transistors would be mounted and the irradiation chamber was assembled as outlined earlier and lowered into the irradiation tube. The wires were irradiated for one hour at 100 kW power setting. The activities of wires were measured by Canberra high purity germanium detectors and the neutron differential flux was calculated using the SNL-SAND-II code. Measured flux is shown in Figure 8. Using the GaAs damage function in Figure 9, the equivalent 1 MeV GaAs neutron fluence or flux was calculated as described in ASTM 722. Assuming that the neutron spectrum scales linearly with the reactor power the resulting differential total flux at full power (495 kW) was 1.4 $x10^{11}$ nv or 5.74$x10^{10}$ 1 MeV equivalent GaAs neutrons/cm^2 s.

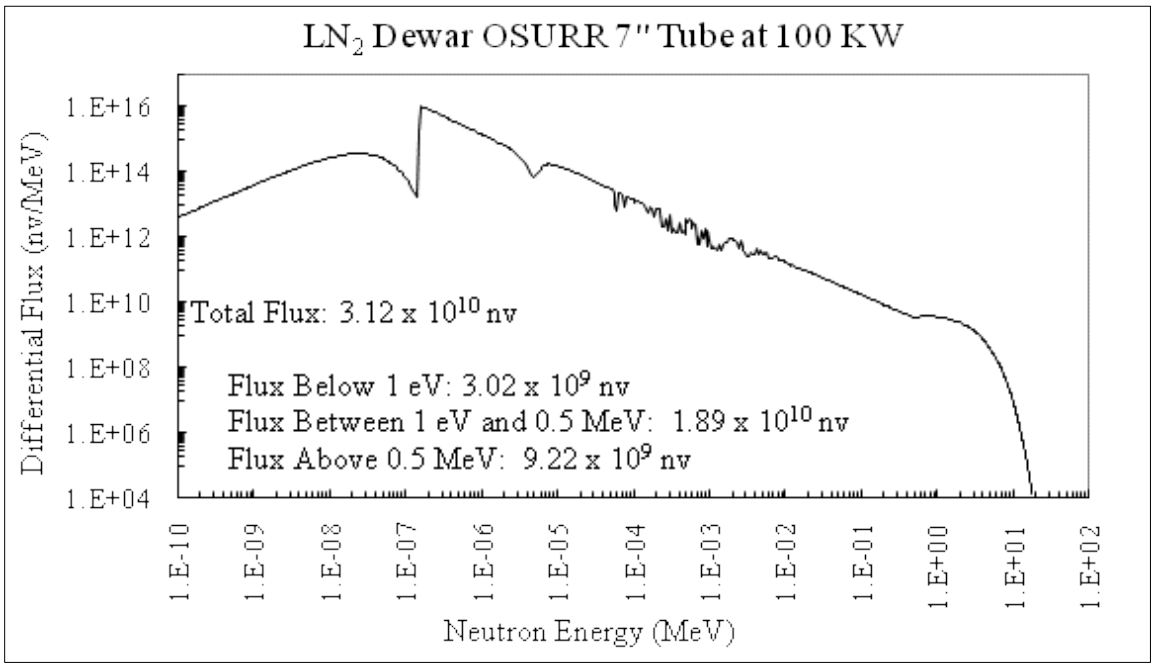

Figure 8. Differential flux neutron spectrum measured inside the new irradiation chamber. A sharp drop off in thermal neutron flux can be seen as a result of 1 mm cadmium shielding.

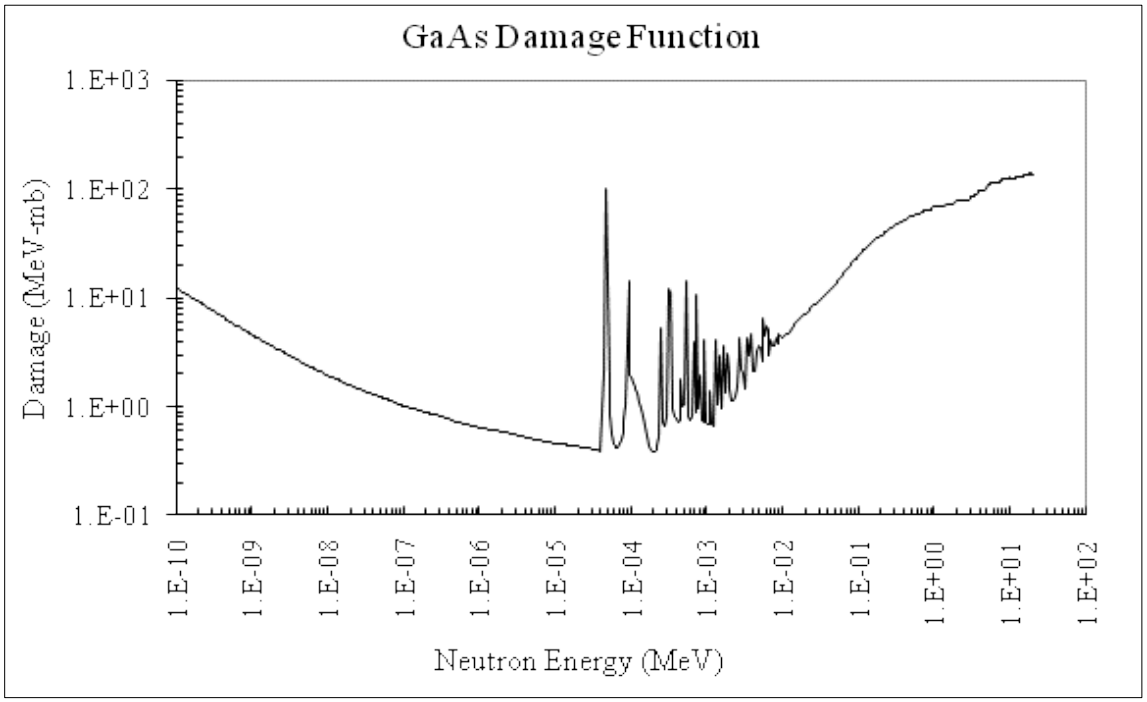

Figure 9. GaAs damage function vs. neutron energy as defined in ASTM 722.

3. Device Manufacturing and Preparation

The AlGaN/GaN wafers were produced by Cree Inc. using the metal-organic vapor-phase epitaxy (MOVPE) method on a 413 μm 4H silicon carbide (4H-SiC) layer. A 2 μm layer consisting of proprietary nucleation and GaN film were deposited on top of the 4H-SiC substrate and a 25 nm $Al_{0.27}Ga_{0.73}N$ layer on top of the GaN layer. The HFETs were produced from wafers by the Air Force Research Laboratory (AFRL) Sensor Directorate. A series of HFETs was deposited on a reticle along with a FATFET. The FATFETs were specifically designed for irradiation studies. FATFETs have longer gate regions (50 μm versus ~ 1 μm) then regular HFETs. This increase in the cross section makes them more susceptible to radiation damage. The ohmic contacts were deposited using layers of titanium, aluminum, nickel and gold of these thicknesses: 3500 Å , 2300 Å, 500 Å and 200 Å, respectively. The Schottky contact was a 200 Å layer of nickel and 2800 Å of gold. The device along with its cross section is shown in Figure 10. Both passivated and un-passivated HFETs were used for this study. Passivated HFET have a 150 nm Si_3N_4 layer deposited between the drain-gate and source-gate regions. The AlGaN and GaN layers are undoped. As specified by the manufacturer, at room temperature the nominal carrier concentration was $1.3x10^{13}$ cm^{-2} and the mobility of carriers in the 2DEG was 1300 cm^2/V s.

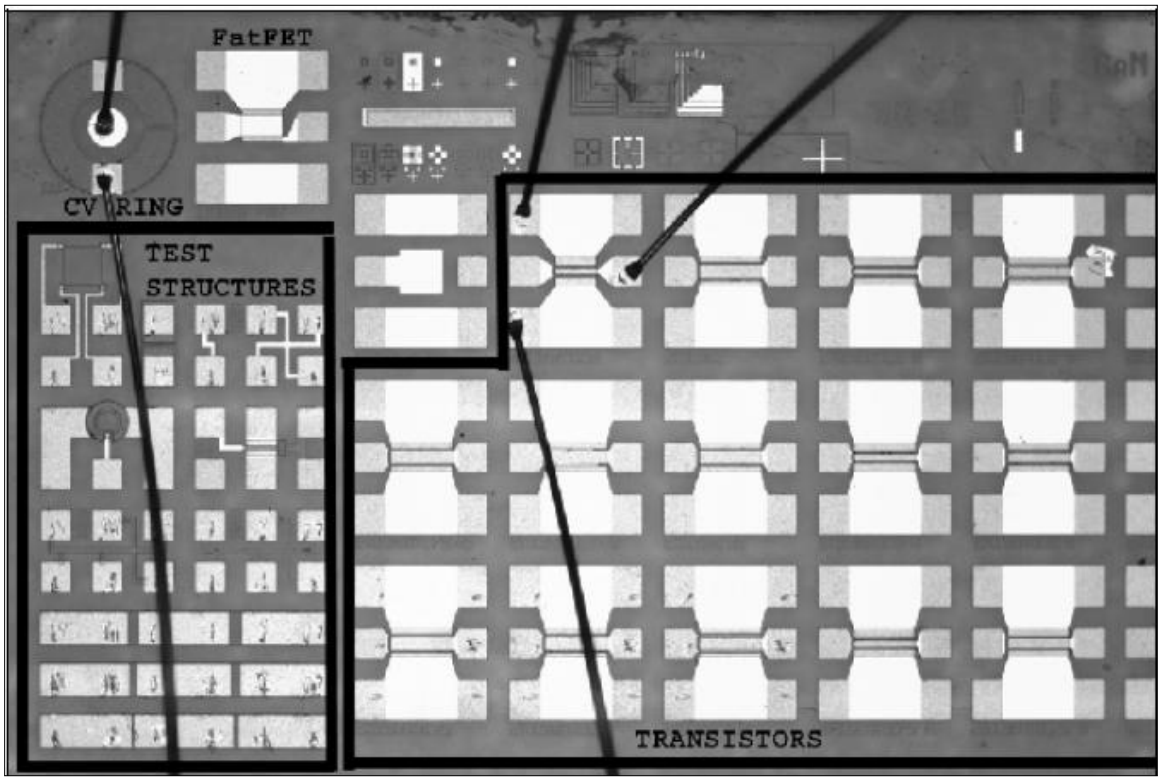

Figure 10. Devices deposited on an AlGaN/GaN wafer. FATFETs were used in this research due to increased vulnerability to radiation.

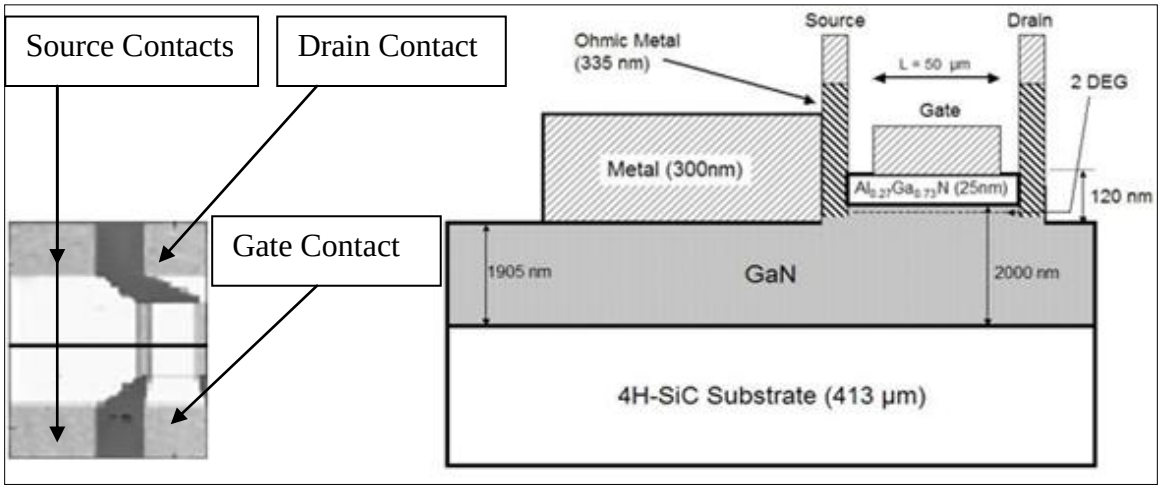

Figure 11. Top view of an HFET with the cross section line and contacts (left). The cross section of the transistor is shown on the right with actual dimensions of devices used in this experiment.

4. Test Setup

Figure 12 shows the basic connections of the data acquisition systems and devices. The HFETs were mounted on a sample holder in the top part of the cold finger. The bottom part of the cold finger was submerged in a glass Dewar filled with liquid nitrogen. A thermocouple (TC) was attached to the back of the cold finger to monitor the temperature of the cold finger and connected to an Omega CNi16D22-EI temperature controller. To prevent condensation forming on the surface of electrical contacts and causing shorts, the HFETs were encapsulated in foam. Since two devices were tested during each run, a total of six cables were used to connect the HFETs to the switching matrix. Cables were connected to the HFETs and tied to the handle to prevent accidental cable pull. RG/62U cables were selected to connect the HFETs and the test matrix. The main reason for selecting these cables was low attenuation of signal at 1MHz used for the gate capacitance measurements over the 25' cable length. RG/58U and RG/174 cables were also considered mainly due to smaller size and mass which would have decreased neutron activation. Unfortunately, due to the distance requirement posed by the design of the reactor those cables were inadequate in propagating the signal through this length. Without the RG/62U cables the 4200 SCS would not have calibrated properly and the capacitance measurements would have been erroneous. Finally, a cadmium tube was put in place to cover the cold finger assembly with the HFETs and after ensuring proper device response the irradiation chamber was lowered into the 7" irradiation tube.

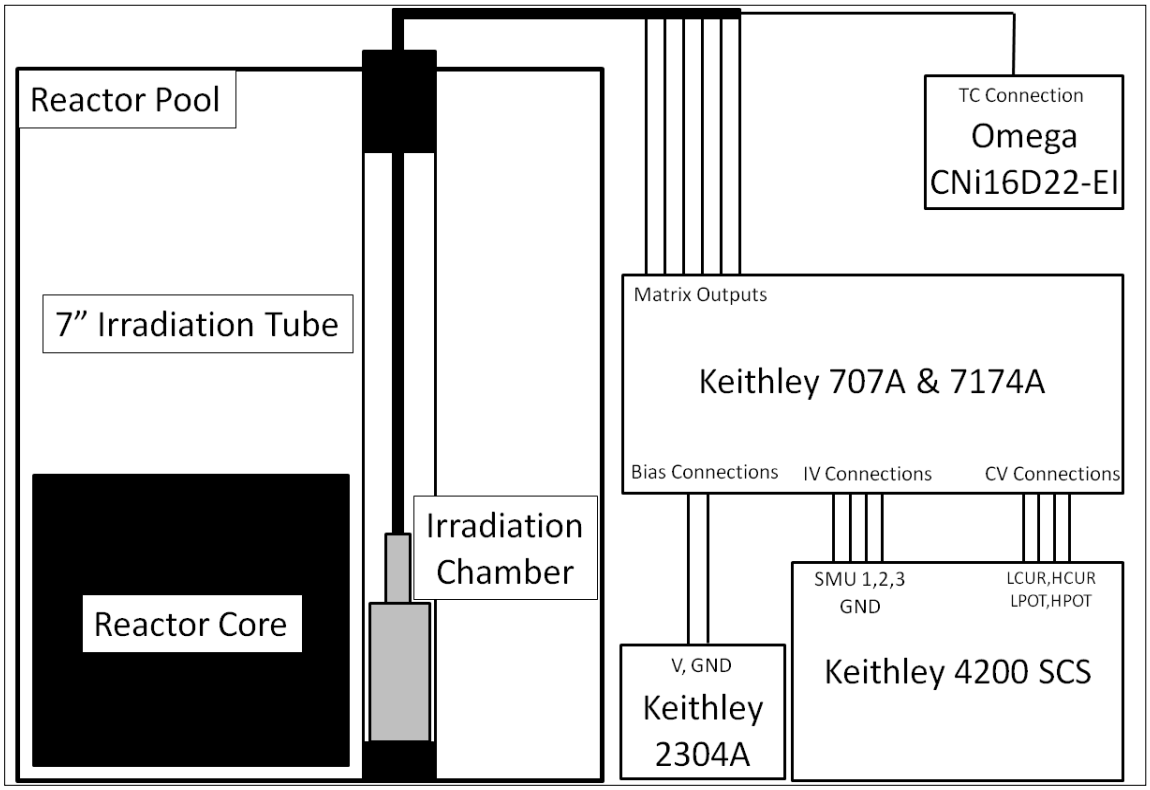

Figure 12. Test setup shows basic connections between the data acquisition system.

5. Calibration Procedures

To maintain accurate data acquisition, the source-measure unit calibration of the acquisition system (Keithley 4200 SCS) was performed as outlined in the reference manual, every 24-hours or when the temperature change more than 1 degree. Similarly, connection compensation was performed in accordance with the manufacturer’s instructions to ensure correct capacitance measurements. All calibrations and compensations were performed using the “test ready” setup, meaning the switching matrix with cables were attached and the matrix had proper row-column connected to propagate signals through the cables used in this study.

Although all six cables used to connect the transistors to the switching matrix were of the same type and length, there was a small error introduced to the measurement accuracy. After calibrating the 4200 SCS using cables 1,2 and 3, measurements were taken to compare the differences between cables 1,2,3 (used to connect unbiased transistor) and 4,5,6 (used to connect biased transistor). The most extreme recorded differences between the two sets of cables were less than 5% for the capacitance measurements, and less than 2% for transistor current measurements. All devices tested in this experiment were always connected using the same cables therefore the precision of all measurements should be the same. To estimate the precision of measurements, twenty measurements were taken of an HFET produced from the same wafer as devices in this study. Again, the test ready setup was used. The leakage current (V_{gs} = -4 V) relative error was less than 1.5%. The threshold voltage and transistor current errors (V_{ds} = 4 V) were below 0.5%. No corrections were made to compensate for temperature changes inside the irradiation tube. It was assumed that the temperature changes inside the 7" tube due to reactor core heating were not significant and caused no major changes in cable impedance. Although measuring the temperature inside the reactor is complicated due to thermocouple activation and not having temperature sensors near the location of the 7" irradiation tube some assumptions can be made. In this study the temperature sensor was placed just above the reactor core. The temperature reading at 50% power was 95 °F representing the water temperature in the vicinity of the reactor core. This was about 10 °C higher than room temperature (25 °C) as defined in this study.

This temperature increase did not have a significant impact on the I-V and C-V measurement accuracy and precision.

6. Measurements

This section explains the type and significance of electrical measurements taken pre-irradiation, in-situ, post-irradiation and post-annealing period. The test matrix is shown below in Figure 13. One of the objectives of this research was to investigate the effects of gate bias during irradiation on electrical performance of the HFETs. Therefore, samples which were kept under bias during irradiation and during annealing are simply labeled biased, others are referred to as unbiased. Negatively biasing the gate counters the field created by polarization and effectively shuts down the 2 DEG once the negative bias exceeds the threshold voltage. The gates of transistors U10 and U11 were biased with -4 V. It was realized later that irradiation lowered the threshold voltage below -4 V, therefore in subsequent testing the negative biased was increased to -5 V to ensure complete gate closure during irradiation. A total of ten HFETs were tested, eight passivated (U09, U10, U05, U11, JM13, JM111, U092 and U112) and two unpassivated (P03 and P04). Transistors were tested in pairs (sets), one was unbiased and the other biased during irradiation in order to compare their performance under the same testing conditions: neutron flux, environment temperature and device orientation.

Device #	PRE_IRRADIATION				IRRADIATION (LNT)		POST_IRRADIATION			POST_ANNEALING		
	Thermal Break-In	LNT	ΔT=4K	RT	Fluence (neutrons/cm^2) 1MeV equivalent GaAs	Measurement	LNT	ΔT=4K	RT	LNT	ΔT=4K	RT
U09	1 cycle	I_{ds}-V_{ds}		I_{ds}-V_{ds}	9.53E+09	I_{ds}-V_{ds}	I_{ds}-V_{ds}		I_{ds}-V_{ds}	I_{ds}-V_{ds}		I_{ds}-V_{ds}
		I_{gs}-V_{gs}	I_{gs}-V_{gs}-T	I_{gs}-V_{gs}	1.07E+12	I_{gs}-V_{gs}	I_{gs}-V_{gs}	I_{gs}-V_{gs}-T	I_{gs}-V_{gs}	I_{gs}-V_{gs}-T	I_{gs}-V_{gs}-T	I_{gs}-V_{gs}
		I_{ds}-V_{gs}	I_{ds}-V_{gs}-T	I_{ds}-V_{gs}	1.25E+13	I_{ds}-V_{gs}	I_{ds}-V_{gs}	I_{ds}-V_{gs}-T	I_{ds}-V_{gs}	I_{ds}-V_{gs}-T	I_{ds}-V_{gs}-T	I_{ds}-V_{gs}
		C_{gs}-V_{gs}		C_{gs}-V_{gs}	4.75E+13	C_{gs}-V_{gs}	C_{gs}-V_{gs}		C_{gs}-V_{gs}	C_{gs}-V_{gs}		C_{gs}-V_{gs}
U10 (Biased -4V)					1.91E+10	1.91E+11	3.88E+13	2.12E+13	5.63E+13	6.50E+13	7.38E+13	
U05	1 cycle	I_{ds}-V_{ds}		I_{ds}-V_{ds}	9.53E+09	I_{ds}-V_{ds}	I_{ds}-V_{ds}		I_{ds}-V_{ds}	I_{ds}-V_{ds}		I_{ds}-V_{ds}
		I_{gs}-V_{gs}-T	I_{gs}-V_{gs}-	I_{gs}-V_{gs}	1.07E+12	I_{gs}-V_{gs}	I_{gs}-V_{gs}-T	I_{gs}-V_{gs}-T	I_{gs}-V_{gs}	I_{gs}-V_{gs}-	I_{gs}-V_{gs}-T	I_{gs}-V_{gs}
		I_{ds}-V_{gs}-T	I_{ds}-V_{gs}-	I_{ds}-V_{gs}	1.25E+13	I_{ds}-V_{gs}	I_{ds}-V_{gs}-T	I_{ds}-V_{gs}-T	I_{ds}-V_{gs}	I_{ds}-V_{gs}-	I_{ds}-V_{gs}-T	I_{ds}-V_{gs}
		C_{gs}-V_{gs}		C_{gs}-V_{gs}	4.75E+13	C_{gs}-V_{gs}	C_{gs}-V_{gs}		C_{gs}-V_{gs}	C_{gs}-V_{gs}		C_{gs}-V_{gs}
U11 (Biased -4V)					1.91E+10	1.91E+11	3.88E+13	2.12E+13	5.63E+13	6.50E+13	7.38E+13	
JM13	1 cycle	I_{ds}-V_{ds}		I_{ds}-V_{ds}	9.53E+09	I_{ds}-V_{ds}	I_{ds}-V_{ds}		I_{ds}-V_{ds}	I_{ds}-V_{ds}		I_{ds}-V_{ds}
		I_{gs}-V_{gs}-T	I_{gs}-V_{gs}-	I_{gs}-V_{gs}	1.07E+12	I_{gs}-V_{gs}	I_{gs}-V_{gs}-T	I_{gs}-V_{gs}-T	I_{gs}-V_{gs}	I_{gs}-V_{gs}-	I_{gs}-V_{gs}-T	I_{gs}-V_{gs}
		I_{ds}-V_{gs}-T	I_{ds}-V_{gs}-	I_{ds}-V_{gs}	1.25E+13	I_{ds}-V_{gs}	I_{ds}-V_{gs}-T	I_{ds}-V_{gs}-T	I_{ds}-V_{gs}	I_{ds}-V_{gs}-	I_{ds}-V_{gs}-T	I_{ds}-V_{gs}
		C_{gs}-V_{gs}		C_{gs}-V_{gs}	4.75E+13	C_{gs}-V_{gs}	C_{gs}-V_{gs}		C_{gs}-V_{gs}	C_{gs}-V_{gs}		C_{gs}-V_{gs}
JM111 (Biased -5V)					1.91E+10	1.91E+11	3.88E+13	2.12E+13	5.63E+13	6.50E+13	7.38E+13	
U092	1 cycle	I_{ds}-V_{ds}		I_{ds}-V_{ds}	9.53E+09	I_{ds}-V_{ds}	I_{ds}-V_{ds}		I_{ds}-V_{ds}	I_{ds}-V_{ds}		I_{ds}-V_{ds}
		I_{gs}-V_{gs}-T	I_{gs}-V_{gs}-	I_{gs}-V_{gs}	1.07E+12	I_{gs}-V_{gs}	I_{gs}-V_{gs}-T	I_{gs}-V_{gs}-T	I_{gs}-V_{gs}	I_{gs}-V_{gs}-	I_{gs}-V_{gs}-T	I_{gs}-V_{gs}
		I_{ds}-V_{gs}-T	I_{ds}-V_{gs}-	I_{ds}-V_{gs}	1.25E+13	I_{ds}-V_{gs}	I_{ds}-V_{gs}-T	I_{ds}-V_{gs}-T	I_{ds}-V_{gs}	I_{ds}-V_{gs}-	I_{ds}-V_{gs}-T	I_{ds}-V_{gs}
		C_{gs}-V_{gs}		C_{gs}-V_{gs}	4.75E+13	C_{gs}-V_{gs}	C_{gs}-V_{gs}		C_{gs}-V_{gs}	C_{gs}-V_{gs}		C_{gs}-V_{gs}
U112 (Biased -5V)					1.91E+10	1.91E+11	3.88E+13	2.12E+13	5.63E+13	6.50E+13	7.38E+13	
P03	1 cycle	I_{ds}-V_{ds}		I_{ds}-V_{ds}	9.53E+09	I_{ds}-V_{ds}	I_{ds}-V_{ds}		I_{ds}-V_{ds}	I_{ds}-V_{ds}		I_{ds}-V_{ds}
		I_{gs}-V_{gs}-T	I_{gs}-V_{gs}-	I_{gs}-V_{gs}	1.07E+12	I_{gs}-V_{gs}	I_{gs}-V_{gs}-T	I_{gs}-V_{gs}-T	I_{gs}-V_{gs}	I_{gs}-V_{gs}-	I_{gs}-V_{gs}-T	I_{gs}-V_{gs}
		I_{ds}-V_{gs}-T	I_{ds}-V_{gs}-	I_{ds}-V_{gs}	1.25E+13	I_{ds}-V_{gs}	I_{ds}-V_{gs}-T	I_{ds}-V_{gs}-T	I_{ds}-V_{gs}	I_{ds}-V_{gs}-	I_{ds}-V_{gs}-T	I_{ds}-V_{gs}
		C_{gs}-V_{gs}		C_{gs}-V_{gs}	4.75E+13	C_{gs}-V_{gs}	C_{gs}-V_{gs}		C_{gs}-V_{gs}	C_{gs}-V_{gs}		C_{gs}-V_{gs}
P04 (Biased -5V)					1.91E+10	1.91E+11	3.88E+13	2.12E+13	5.63E+13	6.50E+13	7.38E+13	

Figure 13. Test Matrix.

a) Pre-Irradiation Measurements and Device Characterization

As shown in previous research by McClory [15] and Moran [16] at least one thermal break-in measurement cycle was needed to minimize variations in I_{gs}. The thermal break in involves cooling the devices down to 82 K and warming it back up to 294 K. The ohmic contacts are prone to performance variations due to temperature changes and the break-in process effectively reducing variations in performance. As shown by McClory [15] the differences between devices before and after break-in can be as high as 27% in the case of leakage current at 294 K and around 12% at 82 K. In this study the thermal break-in was performed three times. Data was only recorded during the last cycle. These measurements were crucial as they provided the basis to which in-situ, post-irradiation and post-anneal HFET electrical properties were compared.

b) In-Situ Measurements

The in-situ measurements were the main focus of this study. The author is unaware of any existing in-situ studies performed to date on AlGaN/GaN HFETs under neutron irradiation. Four different power setting were selected: 250 W, 2.3 kW, 23 kW and 230 kW. The power ramp up is shown in Figure 14. Measurements were taken after the irradiation chamber was lowered into the tube (before reactor was turned on) and every five minutes afterwards, resulting in readings at sixteen fluence levels. The temperature changes inside the 7” irradiation tube were not accounted for. It was assumed that the temperature changes would not have affected the resistance of cables to cause significant errors in voltage and current measurements as stated earlier.

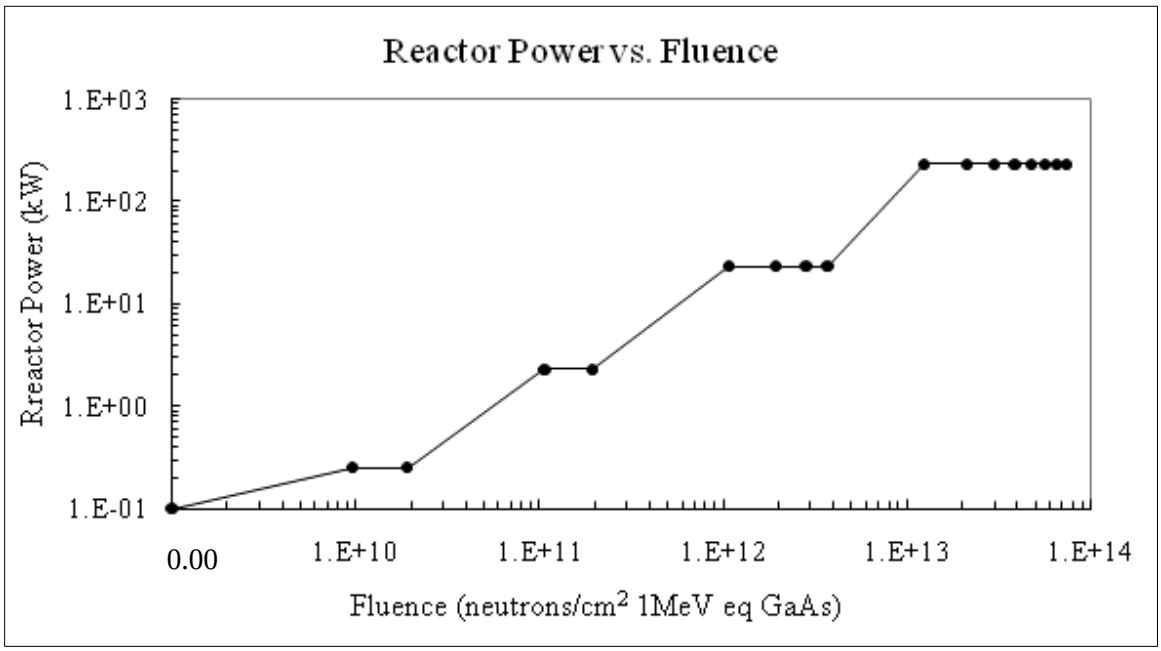

Figure 14. Reactor Power ramp up. Dots represent fluences at which measurements were taken.

c) Post-Irradiation Measurements

Following the irradiation, the samples were left inside the irradiation tube for 1.5 hours to allow for the decay of short lived isotopes. Next, the irradiation chamber was pulled out of the tube and the cold finger with HFETs was transferred to a different liquid nitrogen filled Dewar and cooled to a minimum possible temperature. Measurements were taken as the liquid nitrogen was evaporating allowing the cold finger and devices to warm up slowly. Measurements were taken in steps of 4 K.

d) Post-Annealing Measurements

Post-annealing measurements were performed after the HFETs had remained at 300 K for 21 days after irradiation. Four transistors (U09, U10, U05 and U11) were not biased during this period, remaining six (JM13, JM111, U092, U112, P03 and P04) had

gate bias of -5 V with respect to source. Post annealing measurements were taken in steps of 4 K from 77 K to 300 K.

e) Gate-Source Capacitance vs. Gate-Source Voltage (C_{gs}-V_{gs})

Measuring gate capacitance provides information about the interface trap formation. With the drain voltage at 0 V, the source voltage was swept from -6 to 0 V in steps of 0.1 V. These measurements were recorded at 77 K and 300 K as well as pre, in-situ, post-irradiation and post-annealing period.

f) Drain-Source Current vs. Drain-Source Voltage (I_{ds}-V_{ds})

These measurements were used to investigate the sheet charge density and carrier mobility. Pre, in-situ and post irradiation transistor currents were compared. Data was taken at 77 K and 300 K. The gate voltage was stepped from 0 to -4 V in 1 V increments, the source was kept at 0 V and the drain voltage was swept from 0 to 8 V in steps of 0.1 V.

g) Temperature Dependent Drain-Source Current vs. Gate-Source Voltage (I_{ds}-V_{gs}-T)

This type of measurement was used to observe the changes in threshold voltage, V_{th}, as a function of temperature pre, in-situ, post-irradiation and post-annealing. Measured threshold voltage shifts were used in calculations of carrier mobility and sheet charge concentration. Two methods of measuring the V_{th} were used, the linear extrapolation and transconductance method. The source voltage was kept at 0 volts, 0.2 V was applied to the drain and the gate voltage was swept from -7 to 0 V in steps of 0.1 V. The drain current and transconductance were recorded at 4 K increments from 77 K to 300 K.

h) Temperature Dependent Gate-Source Current vs. Gate-Source Voltage (I_{gs}-V_{gs}-T)

These measurements were taken in order to investigate the interface trap formation and their effect on the trap-assisted-tunneling (TAT) current. The gate leakage current versus gate-source voltage was measured every 4 K from 77 K to 300 K. The gate-source voltage was swept from -4 to 0 V in 0.1 V steps. Pre, in-situ, post-irradiation and post-annealing results were recorded.

V. Experimental Results

Four types of measurements are presented in this chapter: transistor current, I_{ds}, threshold voltage, and leakage current as a function of fluence. Additionally pre and post-irradiation C-V measurements are presented. Due to the failure of 8 out of 10 devices no post anneal measurements are reported. One of the objectives of this study was investigating the effects of biasing the gate during irradiation on these electrical characteristics of the HFETs, Therefore, the devices which were under bias during irradiation are referred to as biased and others unbiased. All devices followed the same trends therefore the averages were calculated and subsequent discussion and analysis was carried out using average values, unless specified otherwise.

1. Drain Conductance (g_d) vs. Fluence

The drain conductance was derived from I_{ds} measurements using equation (10) and evaluated at V_{ds} = 0 V. The results for unbiased and biased devices are plotted in Figure 15 and Figure 16, respectively. Due to variations in devices the results were averaged and the differences were compared as relative changes in average values. The drain conductance, g_d, initially increased ~6% from the pre-irradiation value and remained constant until it started to drop off at higher fluences 10^{13} neutrons/cm^2. The drop in conductance during irradiation was <5% in unpassivated devices (unbiased and biased). The drain conductance in unbiased passivated HFETs increased ~2% from pre-irradiation value and similarly to unpassivated devices started decreasing at 10^{13} n/cm^2. The maximum relative decrease in conductance in the passivated HFETs was ~5%, practically the same as in unpassivated HFETs.

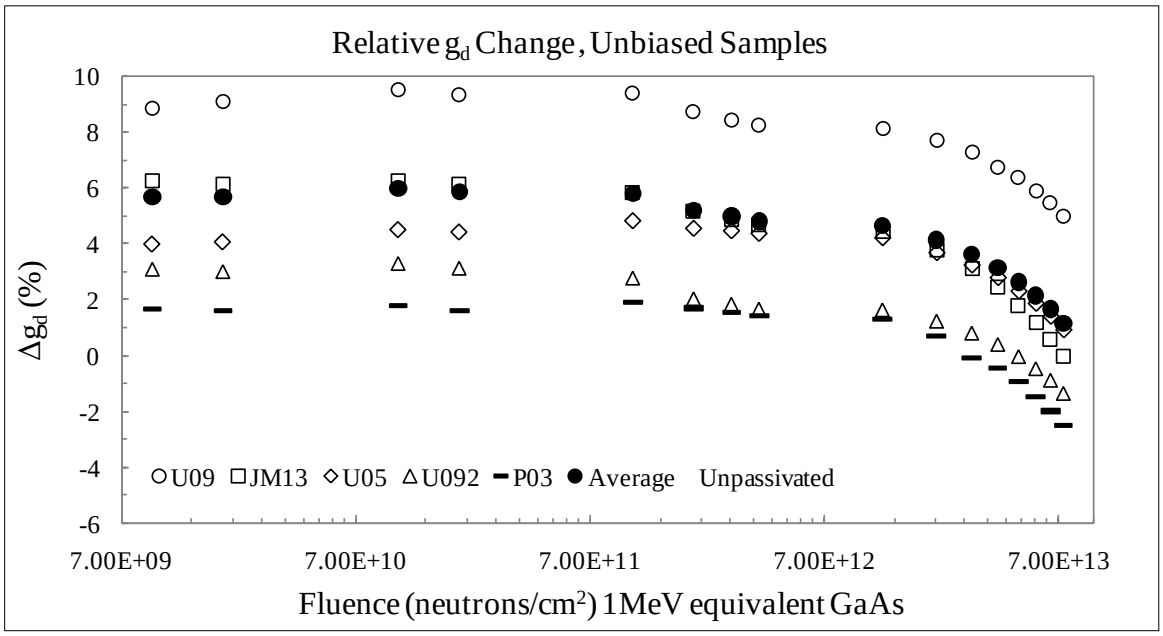

Figure 15. Relative drain conductance changes vs. fluence in unbiased samples.

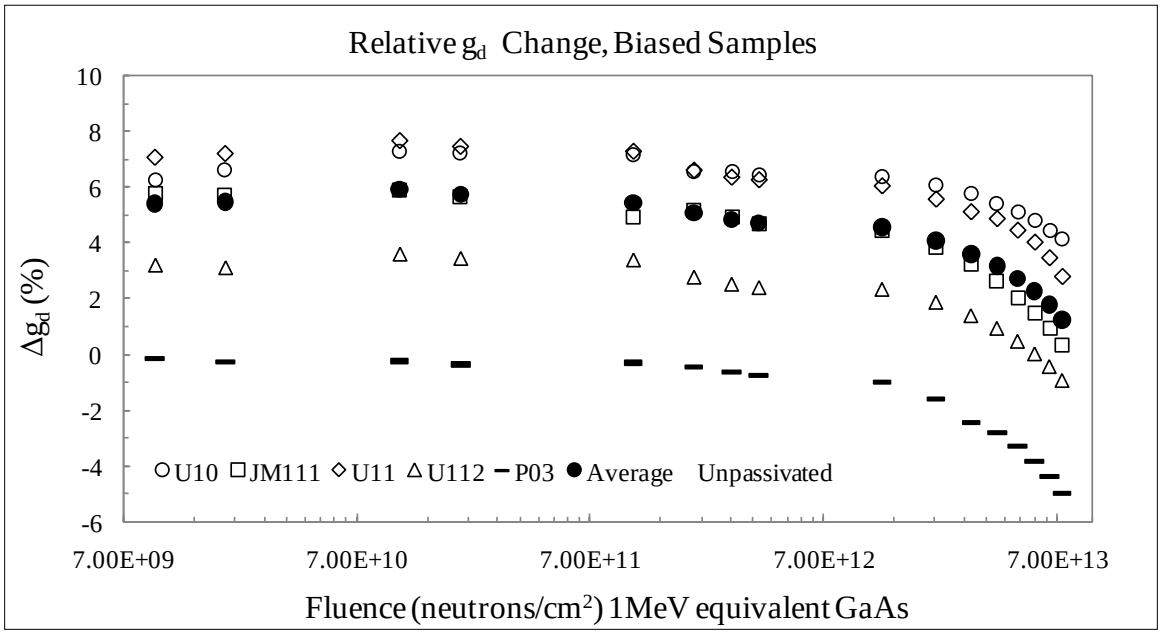

Figure 16. Relative drain conductance changes vs. fluence in biased samples.

2. Transistor Current (I_{ds}) vs. Fluence

A noticeable change in transistor current was observed during irradiation as compared to the pre-irradiation values in unpassivated, unbiased transistors. After the initial increase of ~12% from the pre-irradiation level the transistor current slowly increased and peaked at ~14% at a fluence of 1.25×10^{13} neutrons/cm^2. After that total fluence, the current started dropping gradually as shown in Figure 17. This drop continued even after the reactor was shut down and the irradiation chamber was removed from the irradiation tube. All, but two transistors failed within a few hours after irradiation therefore no post annealing comparison is presented. Figure 18 shows the same results for biased samples. Although the current changes were different among all sets of HFETs, no significant difference was observed in 3 sets (U09 & U10, U092 & U112, JM13 & JM111) of unpassivated devices between the biased and unbiased transistors.

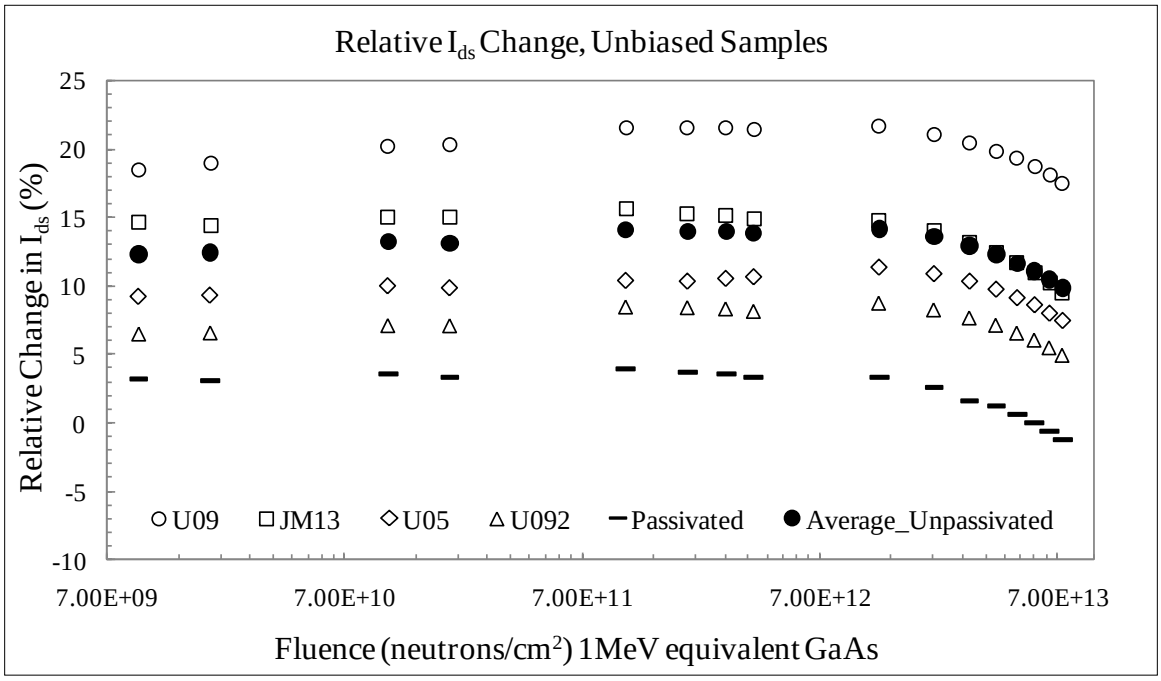

Figure 17. Relative current change in unbiased samples.

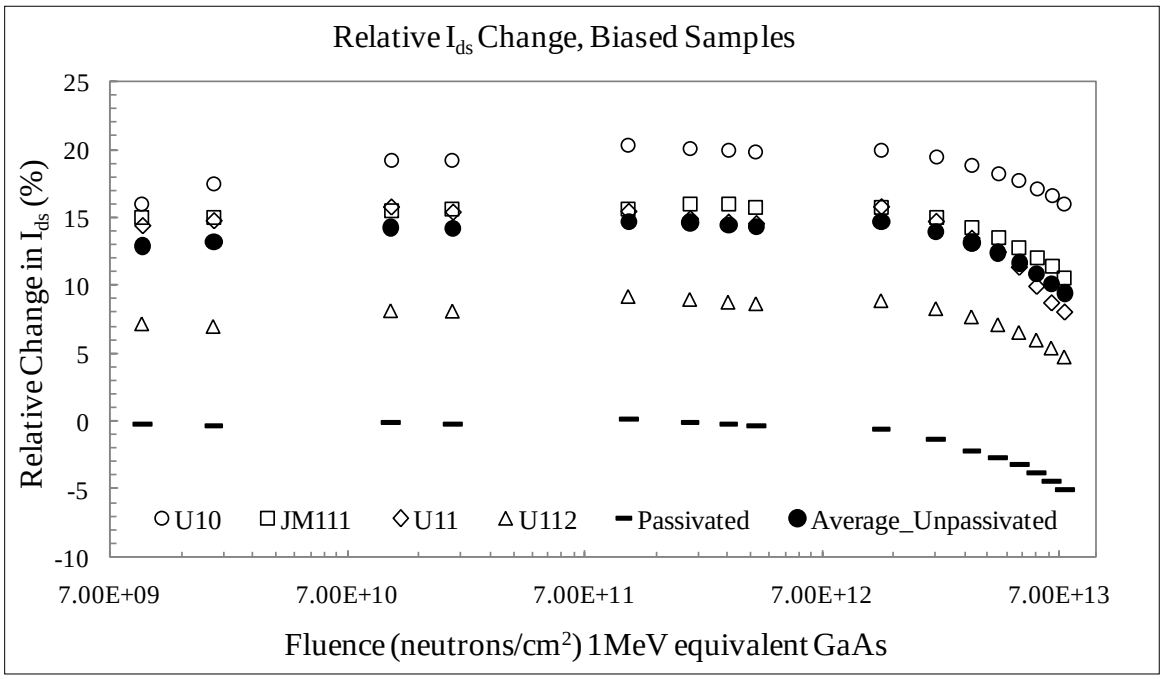

Figure 18. Relative current change in biased samples.

The maximum current change was ~11% in the unbiased U05 transistor versus ~16% in the biased U11 device. The difference between the average change in I_{ds} for biased vs. unbiased devices was less than 5%, which is within the uncertainty of the measurements. Therefore, it can be said that no significant difference in I_{ds} was observed between the biased and unbiased devices.

The unbiased, passivated devices behavior was very similar to that of unbiased, unpassivated HFETs. The increase from pre-irradiation I_{ds} measurement, although smaller (~4%), was seen initially followed by a gradual drop off starting at a fluence of 1.25×10^{13} neutrons/cm^2. The biased device (P04) did not show any significant change in I_{ds} until the fluence reached 1.25×10^{13} neutrons/cm^2. At that point the current started dropping below the pre-irradiation value. The maximum I_{ds} difference between the unbiased HFET, P03, and the biased HFET, P04, never exceeded ~4%. In comparing

unpassivated to passivated HFETs, the unpassivated HFETS demonstrated a much higher increase in I_{ds} during irradiation: ~11% in the case of unbiased and ~15% in the case of biased HFETs. This result suggests that the passivation layer minimizes the I_{ds} current increase during neutron irradiation.

3. Threshold Voltage (V_{th}) vs. Fluence

The threshold voltage in unpassivated (both unbiased and biased) devices increased in absolute value from the pre-irradiation values, as shown in Figure 19 and Figure 20. The first measurement of the threshold voltage shift at a total fluence of 9.53×10^9 neutrons/cm^2) was an increase of 7% and continued to increase slowly up to around 9% until a fluence of 1.7×10^{13} neutrons/cm^2 was reached. At that point the change in V_{th} remained constant, unlike the changes in I_{ds}.

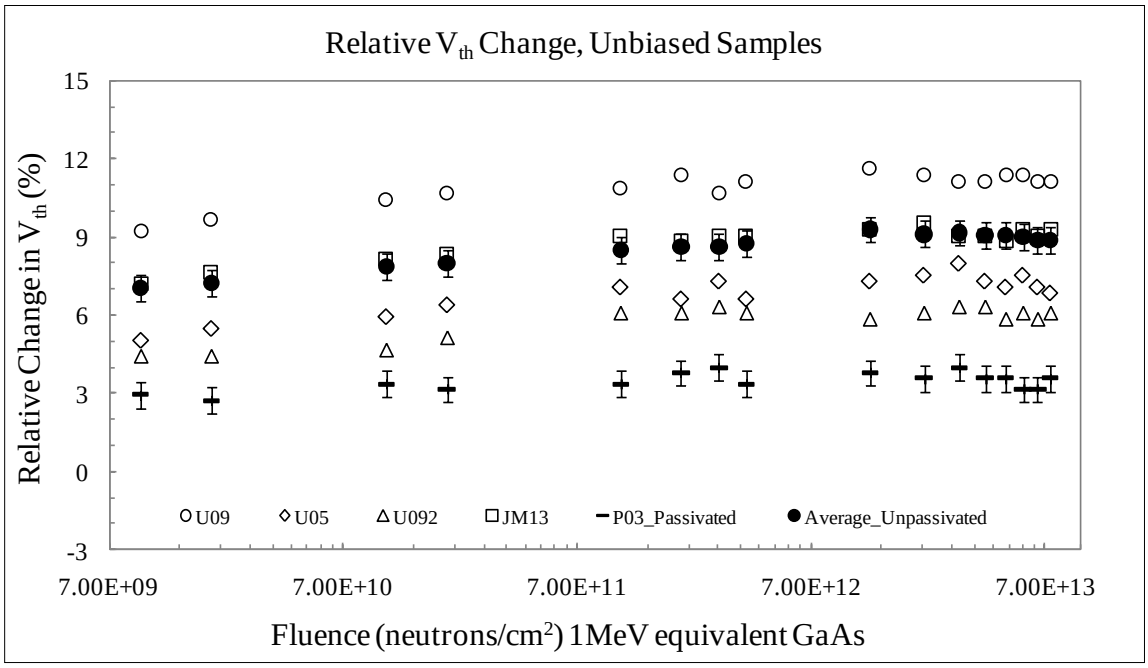

Figure 19. Relative V_{th} Change in unbiased samples.

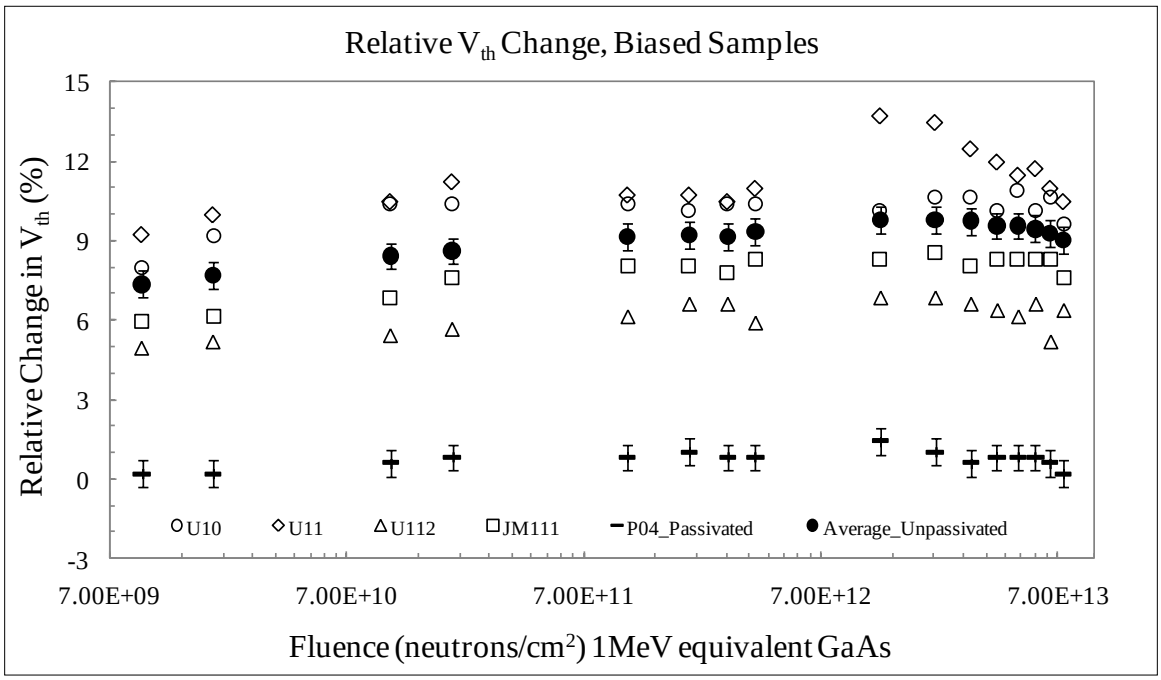

Figure 20. Relative V_{th} Change in biased samples.

A maximum difference of less than 0.5% was observed between unbiased and biased samples threshold voltage shifts under neutron irradiation at corresponding fluences in transistors U09 & U10, U092 & U112, and JM13 & JM111. Averaging V_{th} in unpassivated samples resulted in a maximum difference of less than 0.5% between unbiased and biased HFETs and is statistically insignificant. The percentage change in the threshold voltage of less than 3%, in both the unbiased and biased cases for passivated HFETS is comparable to the percent increase observed for I_{ds}. This larger V_{th} shift in unpassivated devices agrees with the results of previous studies conducted by McClory, et al. [15][16]

4. Gate Capacitance (C_{gs}) vs. Gate Voltage (V_{gs})

The capacitance measurements were taken as described in the experimental procedures section. The two pairs of transistors U09 and U10 and U05 and U11 that were tested first had noisy capacitance measurements. The reason for this interference was not identified, although it disappeared during the second set of tests. All data presented here was corrected for the temperature increase due to evaporation of liquid nitrogen during in-situ measurements. No quantitative analysis of interface trap formation was performed in this study. Results presented here are strictly of qualitative nature and are used to provide evidence for interface trap formation. Figure 21 and Figure 22 show the C-V curves of the unbiased JM13 and biased JM111 devices, respectively.

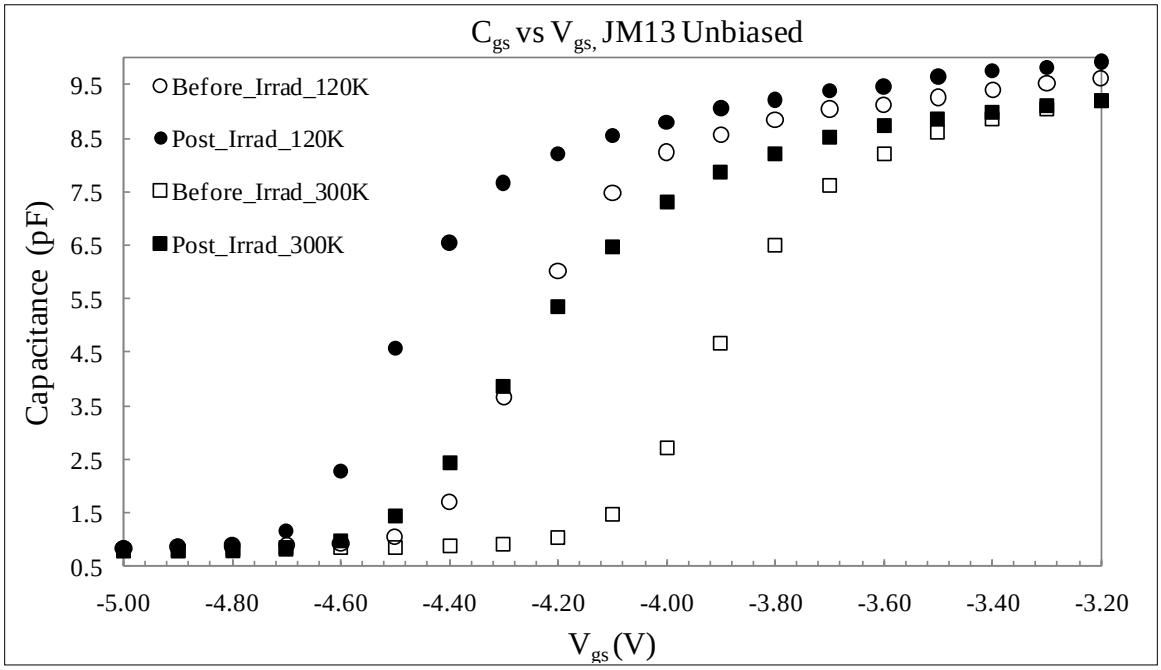

Figure 21. Gate Capacitance versus Gate Voltage, transistor JM13. Flattened slope was observed at 300 K indicating interface trap build up.

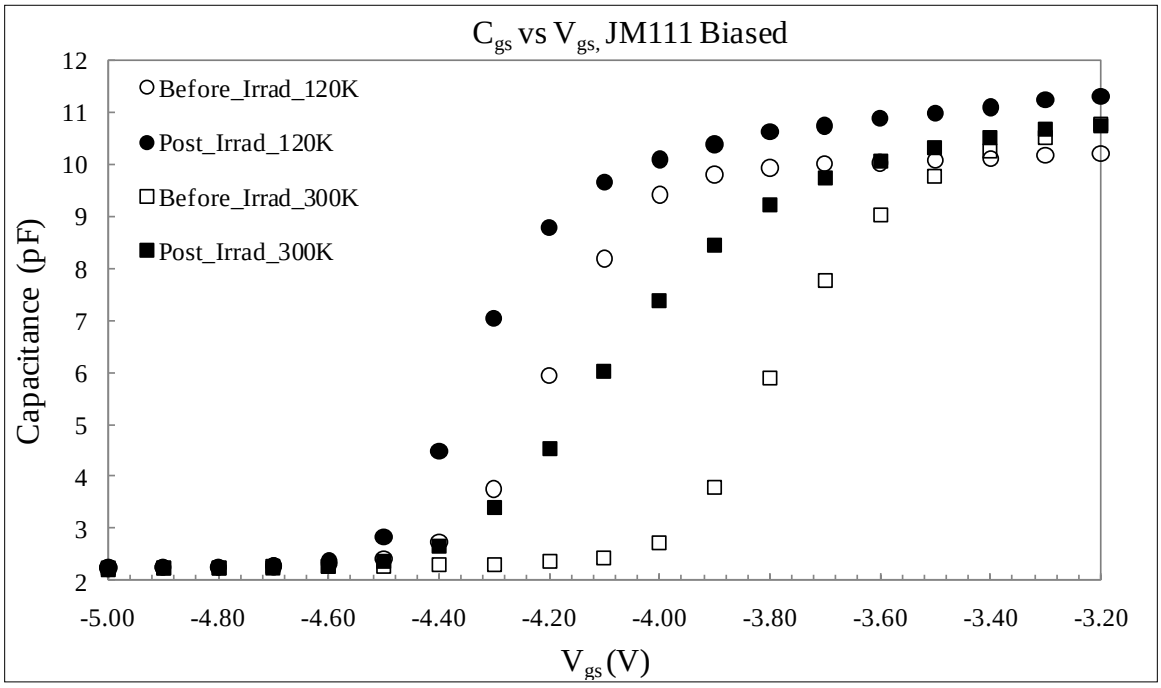

Figure 22. Gate Capacitance versus Gate Voltage, transistor JM111.

The C-V curves shift in negative direction, indicative of positive charge build-up, confirms the threshold voltage shifts presented in Section 3 of this chapter. A change in the slope of the capacitance curve can be seen between the pre and post irradiation 300 K curves indicating a build-up of interface traps during neutron irradiation. At 120 K the interface traps are filled and neutral therefore the difference in slopes between pre and post-irradiation capacitance curves is minimal. At 300 K the traps are ionized and manifest themselves as a stretched out C-V curve [10]. Similar results have been observed by McClory, et al. [15][16].

5. Leakage Current ($I_{leakage}$) vs. Fluence

The initial intent was to measure the leakage current pre irradiation, post irradiation and post anneal from 120 K to 300 K. The in-situ part of measurements was performed

only at 120 K. The primary objective of the in-situ part was to observe the change in $I_{leakage}$ as a function of fluence. No transistors survived the post-anneal period. The leakage current in unpassivated, unbiased devices showed a continuous increase with fluence of ~10% to 13% until a fluence of 1.25×10^{13} neutrons/cm^2 (Figure 23). At that point the leakage current started decreasing slowly. The change from the point the $I_{leakage}$ started decreasing until the reactor was shut down was ~2%. A similar trend was observed in the unpassivated, biased HFETs. Results are presented in Figure 24.

Somewhat different behavior was seen in the passivated, unbiased HFET (Figure 23). The leakage current increased gradually from pre-irradiation values, and peaked at ~9% when a fluence of 1.25×10^{13} neutrons/cm^2 was reached. As fluence continued to increase the leakage current started to decrease and ended up back at the pre-irradiation value at a total fluence of 7.38×10^{13} n/cm^2. The biased HFET's leakage current (Figure 24) showed only a small, < 3%, increase in leakage current from pre-irradiation value until a fluence of 3.7×10^{12} n/cm^2. When a fluence of 1.25×10^{13} n/cm^2 was reached the $I_{leakage}$ increased up to 14 % over its pre-irradiation value.

Overall, the relative change in leakage current in passivated devices was much smaller than that of unpassivated devices, in both unbiased and biased devices. These results indicate that passivation enhances radiation hardness and are consistent with previous studies [15][16].

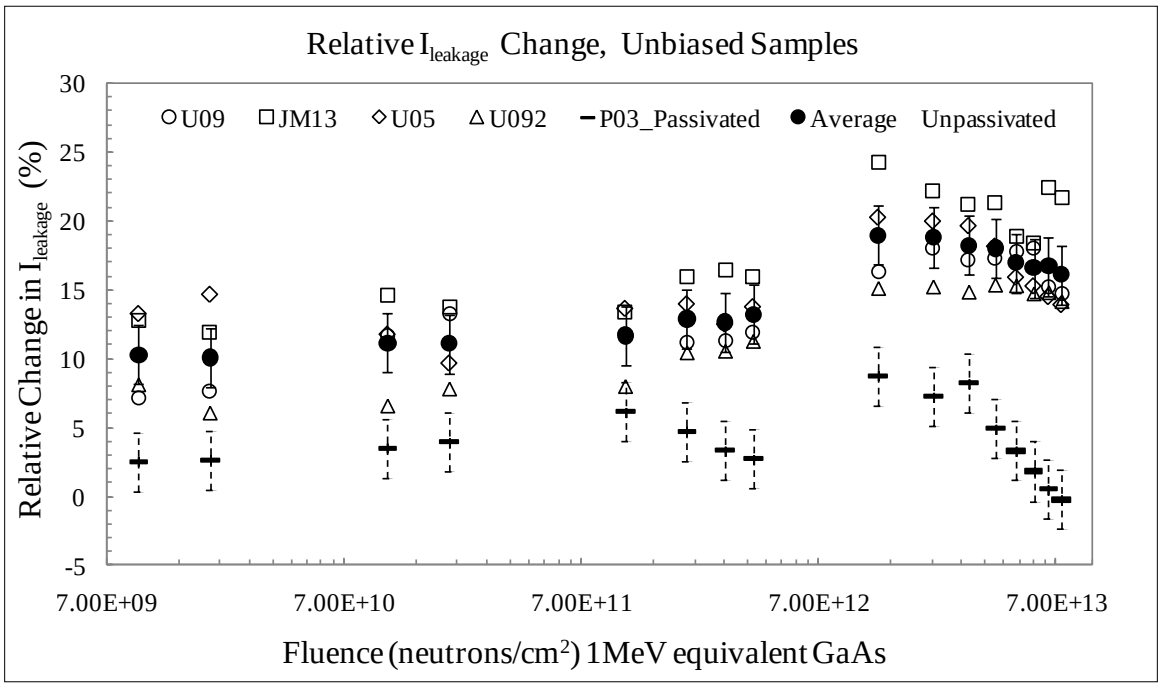

Figure 23. Average leakage current in unbiased samples.

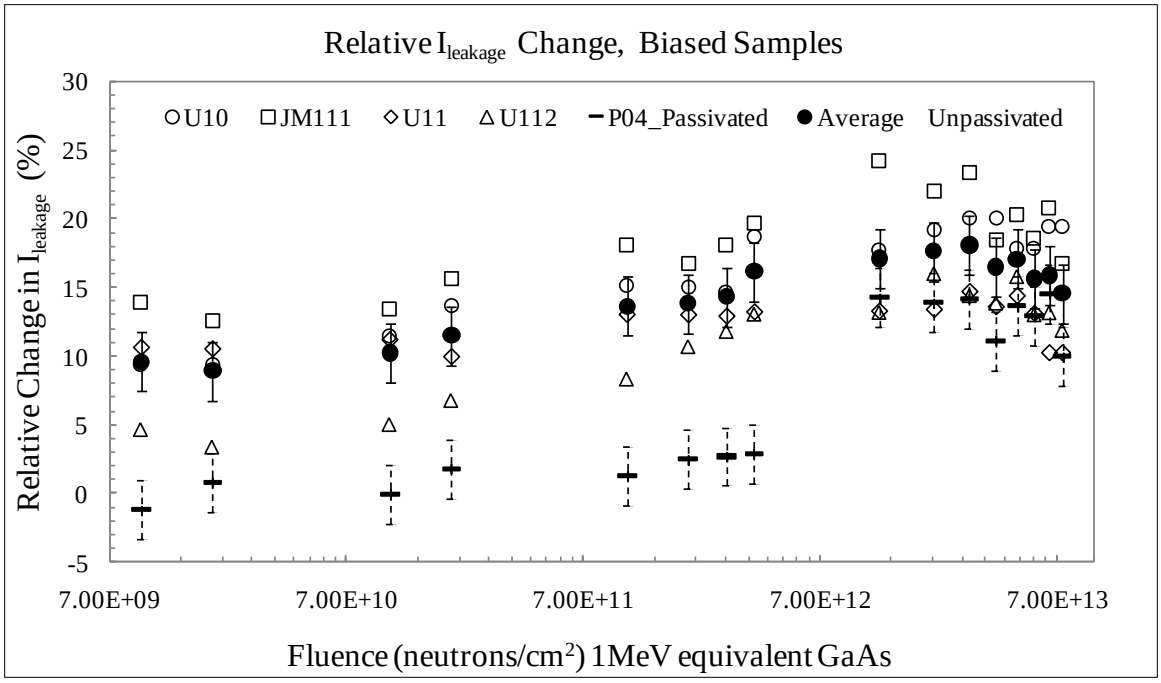

Figure 24. Average leakage current in biased samples.

IV. Analysis of Results

The observed increase over the pre irradiation value of I_{ds} in all unpassivated transistors at low fluence was expected. This increase was much lower in passivated devices. The ions created inside the AlGaN layer by elastic collisions with neutrons travel through the material creating electron-hole pairs. The more mobile electrons are swept to the gate by the fields present in HFETs, both piezoelectric and from the applied bias. The less mobile positive charges are not swept up as quickly and are trapped by displacement damage defects as depicted in Figure 25. These positive charges are immobile at 120 K and result in an increase in the sheet charge concentration. At 300 K the positive charges become mobile and drift towards the interface (creating interface traps) under the influence of the field across the AlGaN layer as shown in Figure 26.

These charges also contribute to the increase in leakage current by lowering the energy barrier for electron tunneling through the AlGaN layer. An increase in sheet charge concentration results in the I_{ds} increase observed in all devices tested in this study (Figure 17 and Figure 18) and is described by equation (21). The positive charge increase inside the AlGaN is further supported by the negative threshold voltage shift (Figure 19, Figure 20), also observed in all HFETs. These positive charges, distributed throughout the AlGaN layer increase the total field, increasing the total concentration of the 2 DEG. Since the threshold voltage is defined as the voltage required to shut off the 2 DEG, the V_{th} naturally has to increase in the negative direction in order to overcome the stronger field resulting from the positive charge increase.

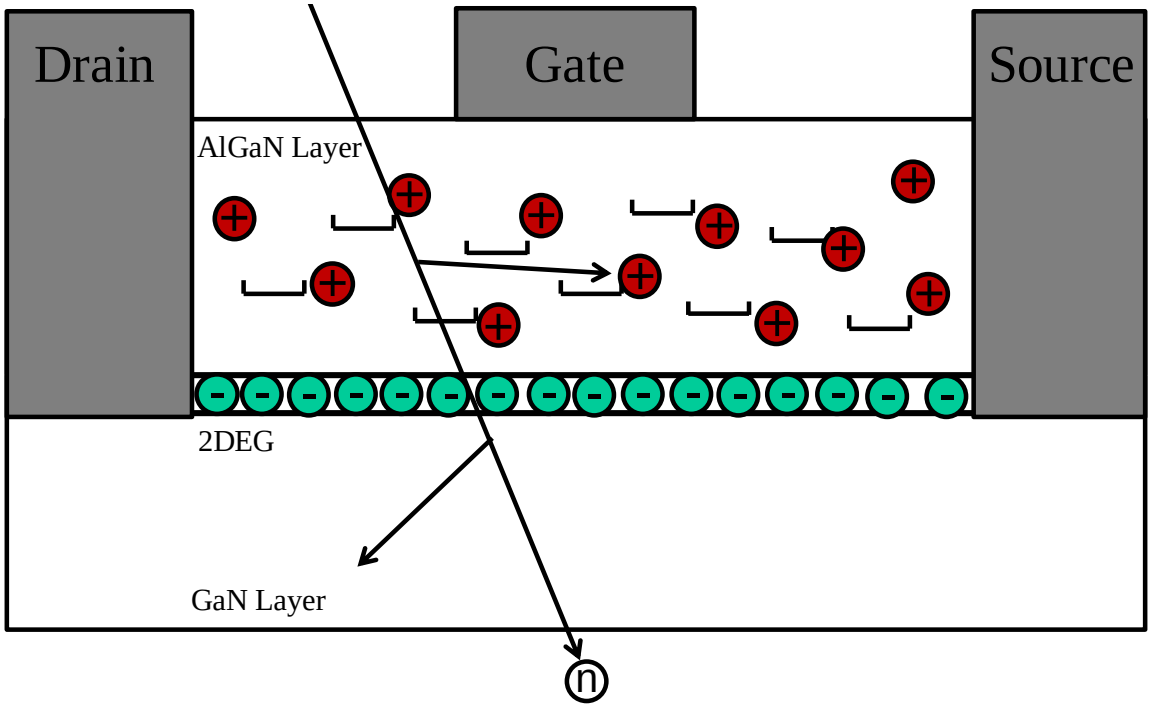

Figure 25. Positive charge creation process as a result of neutron irradiation. Spheres with positive signs represent positive charges. Traps are represented by brackets.

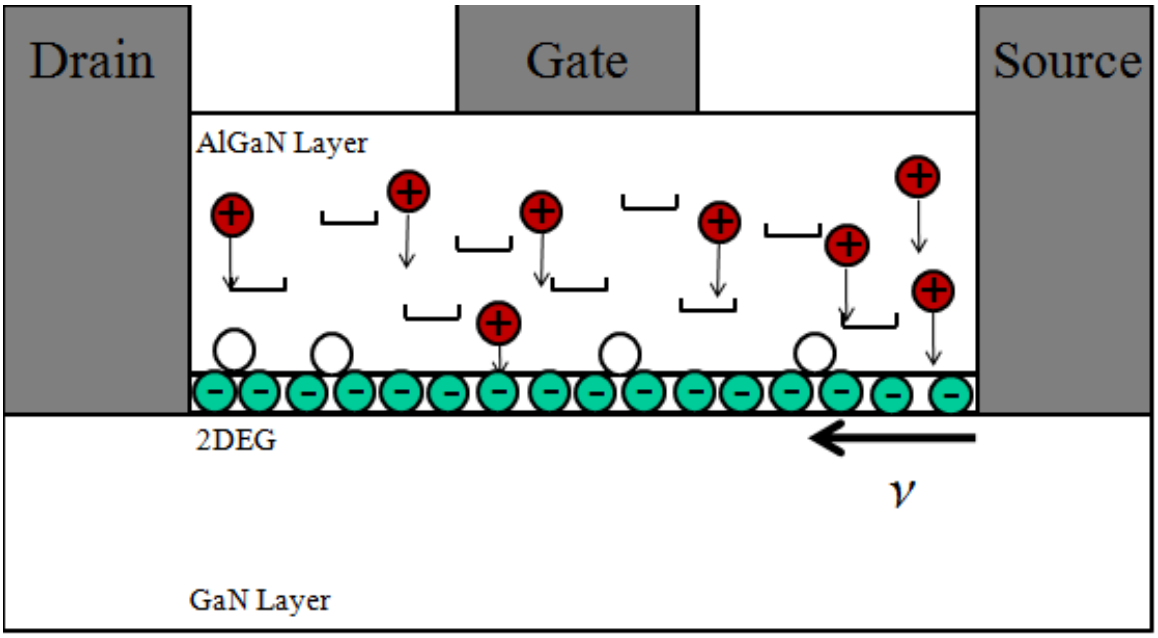

Figure 26. Mobile charge migration towards the interface at 300 K. These mobile charges (circles with a positive sign) turn into interface traps (white circles) and as a result degrade mobility and increase the trap-assisted-tunneling current.

At higher fluences, 1.25×10^{13} n/cm^2, the transistor current started to decrease gradually. Two mechanisms could be responsible for this current drop, carrier removal and mobility degradation. Both mechanisms have been investigated previously [17][18][23][30]. The mobility degradation was found to be a significant factor at fluences above 10^{14} n/cm^2. Significant change in the carrier concentration was observed at fluences of more than two orders of magnitude higher, > 2.4×10^{16} n/cm^2. In this study the maximum fluence reached was <10×14 n/cm^2, therefore mobility degradation was assumed to be the process responsible for the decrease in I_{ds}.

The mobility change with fluence is presented in Figure 27. No significant difference was observed between the biased and unbiased devices. The carrier mobility drops only about 5% during the irradiation period in both biased and unbiased samples.

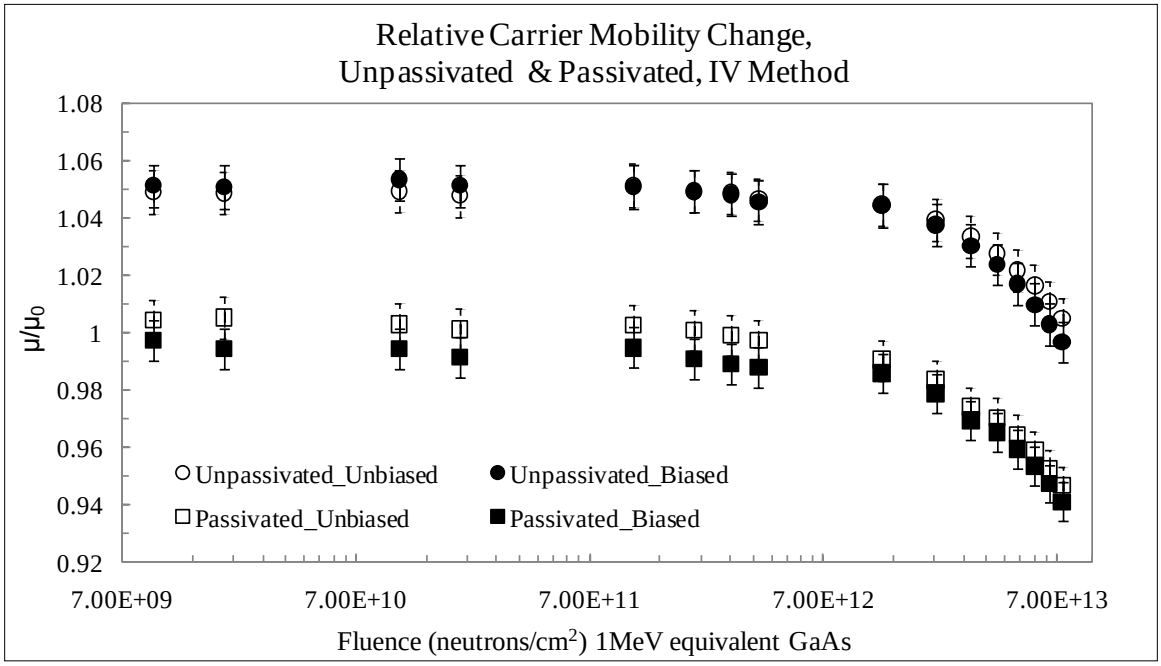

Figure 27. Average carrier mobility of unpassivated and passivated samples.

The proposed mechanism responsible for the mobility decrease is neutron induced damage near the 2 DEG. Neutron displacement damage creates charged defects. These charged defects in GaN near the 2 DEG interact with carriers via Coulombic forces effectively reducing carrier mobility [30]. In addition, the neutrons damage the AlGaN/GaN interface increasing its roughness [31]. The interface roughness in the AlGaN/GaN interface ca be described as variation of the well width or alloy composition. Both, the well width and alloy composition can affect the electron confinement energy [32]. The 2 DEG located inside the GaN layer in proximity to the AlGaN/GaN interface can be affected by the interface roughness and as a result the scattering is further enhanced, especially at lower temperatures [31].

Compiled results for I_{ds}, V_{th}, charge concentration and carrier mobilities in unbiased, unpassivated devices are presented in Table 1. The values of biased, unpassivated samples are shown in Table 2. These sheet charge concentration are on the order of those observed by McClory [15]. He observed a sheet charge concentration of 1.08×10^{12} cm^{-2} with 0.5 V threshold voltage shift. Using the measured changes in V_{th} and I_{ds} the carrier mobility was calculated as described by equations (21)-(24). According to the theory, the mechanism responsible for increasing the threshold voltage is positive charge buildup in the AlGaN layer therefore, the sheet charge density, n_s, was determined using measured threshold voltage and modified equation (24) in this form

$$n_s = \frac{\varepsilon}{qd} (-V_{th}) \tag{26}$$

Table 1. Average values of transistor current, threshold voltage, charge concentration and mobility of unpassivated unbiased devices.

UNPASSIVATED UNBIASED SAMPLES								
Fluence	Ids [A] measured	ΔIds [A] measured	Avg. Vth [V] measured IV	Avg. ΔVth [V] (measured) IV	n_s [cm^{-2}]	Δμ [cm^2/V s]	μ [cm^2/V s]	σ μ
Pre_Irradiation	3.11E-02		-4.23		9.00E+12		5396	38
9.53E+09	3.49E-02	3.83E-03	-4.53	-0.30	9.63E+12	0	5661	40
1.91E+10	3.50E-02	3.87E-03	-4.53	-0.31	9.65E+12	0	5659	40
1.07E+11	3.52E-02	4.11E-03	-4.56	-0.33	9.71E+12	0	5662	40
1.94E+11	3.52E-02	4.09E-03	-4.57	-0.34	9.72E+12	0	5654	40
1.07E+12	3.55E-02	4.39E-03	-4.59	-0.36	9.77E+12	0	5673	40
1.95E+12	3.55E-02	4.35E-03	-4.59	-0.37	9.78E+12	0	5662	40
2.82E+12	3.55E-02	4.34E-03	-4.59	-0.37	9.78E+12	0	5659	40
3.70E+12	3.54E-02	4.30E-03	-4.60	-0.37	9.79E+12	0	5648	40
1.25E+13	3.55E-02	4.41E-03	-4.62	-0.39	9.84E+12	0	5637	40
2.12E+13	3.53E-02	4.23E-03	-4.61	-0.39	9.84E+12	-29	5608	40
3.00E+13	3.51E-02	4.03E-03	-4.62	-0.39	9.84E+12	-61	5576	39
3.88E+13	3.50E-02	3.83E-03	-4.61	-0.38	9.84E+12	-92	5545	39
4.75E+13	3.48E-02	3.63E-03	-4.61	-0.38	9.84E+12	-124	5513	39
5.63E+13	3.46E-02	3.45E-03	-4.61	-0.38	9.84E+12	-153	5484	39
6.50E+13	3.44E-02	3.25E-03	-4.60	-0.38	9.84E+12	-184	5453	39
7.38E+13	3.42E-02	3.06E-03	-4.60	-0.38	9.84E+12	-214	5423	38
Post_Irrad	3.18E-02	6.84E-04	-4.36	-0.13	9.84E+12	-591	5046	36

Table 2. Average values of transistor current, threshold voltage, charge concentration and mobility of unpassivated biased devices.

UNPASSIVATED BIASED SAMPLES								
Fluence	Ids [A] measured	ΔIds [A] measured	Avg. Vth [V] measured IV	Avg. ΔVth [V] (measured) IV	n_s [cm^{-2}]	Δμ [cm^2/V s]	μ [cm^2/V s]	σ μ
Pre_Irradiation	3.16E-02		-4.18		8.90E+12		5537	39
9.53E+09	3.56E-02	4.52E-03	-4.49	-0.31	9.55E+12	0	5821	41
1.91E+10	3.57E-02	4.62E-03	-4.50	-0.32	9.59E+12	0	5819	41
1.07E+11	3.61E-02	4.95E-03	-4.53	-0.35	9.65E+12	0	5834	41
1.94E+11	3.61E-02	4.93E-03	-4.54	-0.36	9.67E+12	0	5821	41
1.07E+12	3.62E-02	5.10E-03	-4.56	-0.38	9.71E+12	0	5819	41
1.95E+12	3.62E-02	5.06E-03	-4.57	-0.39	9.72E+12	0	5810	41
2.82E+12	3.61E-02	5.01E-03	-4.56	-0.38	9.71E+12	0	5804	41
3.70E+12	3.61E-02	4.97E-03	-4.57	-0.39	9.73E+12	0	5789	41
1.25E+13	3.62E-02	5.09E-03	-4.59	-0.41	9.77E+12	0	5783	41
2.12E+13	3.60E-02	4.86E-03	-4.59	-0.41	9.77E+12	-38	5745	41
3.00E+13	3.57E-02	4.60E-03	-4.59	-0.41	9.77E+12	-78	5705	40
3.88E+13	3.55E-02	4.37E-03	-4.58	-0.40	9.77E+12	-114	5669	40
4.75E+13	3.53E-02	4.14E-03	-4.58	-0.40	9.77E+12	-151	5631	40
5.63E+13	3.50E-02	3.89E-03	-4.58	-0.40	9.77E+12	-191	5591	40
6.50E+13	3.48E-02	3.64E-03	-4.57	-0.39	9.77E+12	-230	5553	39
7.38E+13	3.46E-02	3.43E-03	-4.56	-0.38	9.77E+12	-264	5519	39
Post_Irrad	3.19E-02	7.32E-04	-4.25	-0.07	9.05E+12	-692	5091	36

The values for the sheet concentration in this study were computed in the same manner and the carrier mobility was calculated using equation (21) until the fluence of $1.25x10^{13}$ n/cm^2. The highest values of I_{ds} were recorded at that fluence. Since the threshold voltage was calculated using the linear extrapolation technique by measuring I_{ds} [10], which in turn depends on the carrier mobility, calculating the sheet charge concentration past the $1.25x10^{13}$ n/cm^2 fluence using equation (26) would have been erroneous.

It was assumed that the maximum sheet carrier concentration was reached at that point and the subsequent decrease in current was strictly due to mobility degradation. The transistor current, sheet charge concentration and mobility are related by equation (21). Past a fluence of $1.25x10^{13}$ n/cm^2 the change in carrier mobility was estimated by modifying equation (21) into this form

$$\Delta\mu = \frac{\Delta I_{ds}}{q\, W\, E\, n_s} \tag{27}$$

where n_s is the sheet concentration at peak value of I_{ds} and ΔI_{ds} is the change from the peak I_{ds} value at $1.25x10^{13}$ n/cm^2. The resulting change in mobility was then subtracted from the mobility calculated at the fluence when the peak I_{ds} was recorded. Similar changes in mobility were seen in both biased and unbiased passivated devices shown in

Table 3 and

PASSIVATED UNBIASED SAMPLES								
Fluence	Ids [A] measured	ΔIds [A] measured	Avg. Vth [V] measured IV	Avg. ΔVth [V] (measured) IV	n_s [cm^{-2}]	Δμ [cm^2/V s]	μ [cm^2/V s]	μ σ
Pre_Irradiation	4.18E-02		-4.66		9.92E+12	0	6573	46
9.53E+09	4.31E-02	1.35E-03	-4.79	-0.13	1.02E+13	0	6601	47
1.91E+10	4.31E-02	1.30E-03	-4.78	-0.12	1.02E+13	0	6607	47
1.07E+11	4.33E-02	1.47E-03	-4.81	-0.15	1.02E+13	0	6592	47
1.94E+11	4.32E-02	1.40E-03	-4.81	-0.15	1.02E+13	0	6580	47
1.07E+12	4.34E-02	1.64E-03	-4.83	-0.17	1.03E+13	0	6590	47
1.95E+12	4.33E-02	1.55E-03	-4.83	-0.17	1.03E+13	0	6577	47
2.82E+12	4.33E-02	1.49E-03	-4.83	-0.17	1.03E+13	0	6567	46
3.70E+12	4.32E-02	1.40E-03	-4.83	-0.17	1.03E+13	0	6554	46
1.25E+13	4.32E-02	1.38E-03	-4.86	-0.20	1.03E+13	0	6510	46
2.12E+13	4.29E-02	1.07E-03	-4.85	-0.19	1.03E+13	-46	6464	46
3.00E+13	4.24E-02	6.62E-04	-4.84	-0.18	1.03E+13	-108	6402	45
3.88E+13	4.23E-02	4.91E-04	-4.84	-0.18	1.03E+13	-134	6376	45
4.75E+13	4.20E-02	2.39E-04	-4.83	-0.17	1.03E+13	-172	6338	45
5.63E+13	4.18E-02	-9.59E-06	-4.83	-0.17	1.03E+13	-209	6301	45
6.50E+13	4.15E-02	-2.75E-04	-4.82	-0.16	1.03E+13	-249	6261	44
7.38E+13	4.12E-02	-5.37E-04	-4.82	-0.16	1.03E+13	-289	6221	44
Post_Irrad	4.01E-02	-1.65E-03	-4.63	0.03	1.03E+13	-457	6053	43

Table 4.

Table 3. Average values of transistor current, threshold voltage, charge concentration and mobility of passivated unbiased devices.

PASSIVATED UNBIASED SAMPLES								
Fluence	Ids [A] measured	ΔIds [A] measured	Avg. Vth [V] measured IV	Avg. ΔVth [V] (measured) IV	n_s [cm^{-2}]	Δμ [cm^2/V s]	μ [cm^2/V s]	μ σ
Pre_Irradiation	4.18E-02		-4.66		9.92E+12	0	6573	46
9.53E+09	4.31E-02	1.35E-03	-4.79	-0.13	1.02E+13	0	6601	47
1.91E+10	4.31E-02	1.30E-03	-4.78	-0.12	1.02E+13	0	6607	47
1.07E+11	4.33E-02	1.47E-03	-4.81	-0.15	1.02E+13	0	6592	47
1.94E+11	4.32E-02	1.40E-03	-4.81	-0.15	1.02E+13	0	6580	47
1.07E+12	4.34E-02	1.64E-03	-4.83	-0.17	1.03E+13	0	6590	47
1.95E+12	4.33E-02	1.55E-03	-4.83	-0.17	1.03E+13	0	6577	47
2.82E+12	4.33E-02	1.49E-03	-4.83	-0.17	1.03E+13	0	6567	46
3.70E+12	4.32E-02	1.40E-03	-4.83	-0.17	1.03E+13	0	6554	46
1.25E+13	4.32E-02	1.38E-03	-4.86	-0.20	1.03E+13	0	6510	46
2.12E+13	4.29E-02	1.07E-03	-4.85	-0.19	1.03E+13	-46	6464	46
3.00E+13	4.24E-02	6.62E-04	-4.84	-0.18	1.03E+13	-108	6402	45
3.88E+13	4.23E-02	4.91E-04	-4.84	-0.18	1.03E+13	-134	6376	45
4.75E+13	4.20E-02	2.39E-04	-4.83	-0.17	1.03E+13	-172	6338	45
5.63E+13	4.18E-02	-9.59E-06	-4.83	-0.17	1.03E+13	-209	6301	45
6.50E+13	4.15E-02	-2.75E-04	-4.82	-0.16	1.03E+13	-249	6261	44
7.38E+13	4.12E-02	-5.37E-04	-4.82	-0.16	1.03E+13	-289	6221	44
Post_Irrad	4.01E-02	-1.65E-03	-4.63	0.03	1.03E+13	-457	6053	43

Table 4. Average values of transistor current, threshold voltage, charge concentration and mobility of passivated biased devices.

PASSIVATED BIASED SAMPLES								
Fluence	Ids [A] measured	ΔIds [A] measured	Avg. Vth [V] measured IV	Avg. ΔVth [V] (measured) IV	n_s [cm^{-2}]	Δμ [cm^2/V s]	μ [cm^2/V s]	μ σ
Pre_Irradiation	4.36E-02		-4.72		1.00E+13		6764	48
9.53E+09	4.34E-02	1.66E-03	-4.72	0.00	1.00E+13	0	6747	48
1.91E+10	4.34E-02	1.61E-03	-4.73	-0.01	1.01E+13	0	6725	48
1.07E+11	4.35E-02	1.70E-03	-4.74	-0.02	1.01E+13	0	6725	48
1.94E+11	4.35E-02	1.68E-03	-4.75	-0.03	1.01E+13	0	6707	47
1.07E+12	4.36E-02	1.82E-03	-4.75	-0.03	1.01E+13	0	6729	48
1.95E+12	4.35E-02	1.74E-03	-4.76	-0.04	1.01E+13	0	6703	47
2.82E+12	4.35E-02	1.67E-03	-4.76	-0.04	1.01E+13	0	6691	47
3.70E+12	4.34E-02	1.60E-03	-4.76	-0.04	1.01E+13	0	6681	47
1.25E+13	4.33E-02	1.52E-03	-4.77	-0.05	1.01E+13	0	6669	47
2.12E+13	4.30E-02	1.21E-03	-4.77	-0.05	1.01E+13	-61	6620	47
3.00E+13	4.26E-02	7.94E-04	-4.77	-0.05	1.01E+13	-124	6557	46
3.88E+13	4.24E-02	6.14E-04	-4.77	-0.05	1.01E+13	-152	6529	46
4.75E+13	4.21E-02	3.56E-04	-4.76	-0.04	1.01E+13	-192	6489	46
5.63E+13	4.19E-02	9.96E-05	-4.76	-0.04	1.01E+13	-231	6450	46
6.50E+13	4.16E-02	-1.76E-04	-4.76	-0.04	1.01E+13	-274	6407	45
7.38E+13	4.13E-02	-4.52E-04	-4.74	-0.02	1.01E+13	-316	6365	45
Post_Irrad	4.12E-02	-5.40E-04	-4.63	0.09	9.86E+12	-330	6351	45

Figure 28 shows results from similar studies conducted by Polyakov et al. [18] [19]. After irradiating $Al_{0.3}Ga_{0.7}N$/GaN HFETs with 1 MeV neutrons Polyakov observed a 5%

decrease in carrier mobility at a fluence of ~1.4×10^{14} n/cm^2. In this study a 5% change in mobility was observes at ~1.25×10^{13} n/cm^2. Considering the differences between the devices, 0.3 aluminum molar fraction in Polyakov study vs. 0.27 in this study, substrate differences (sapphire vs. silicon carbide) and neutron spectrum (WWR-C vs. LWR reactor), the results in this study were consistent with Polyakov's results.

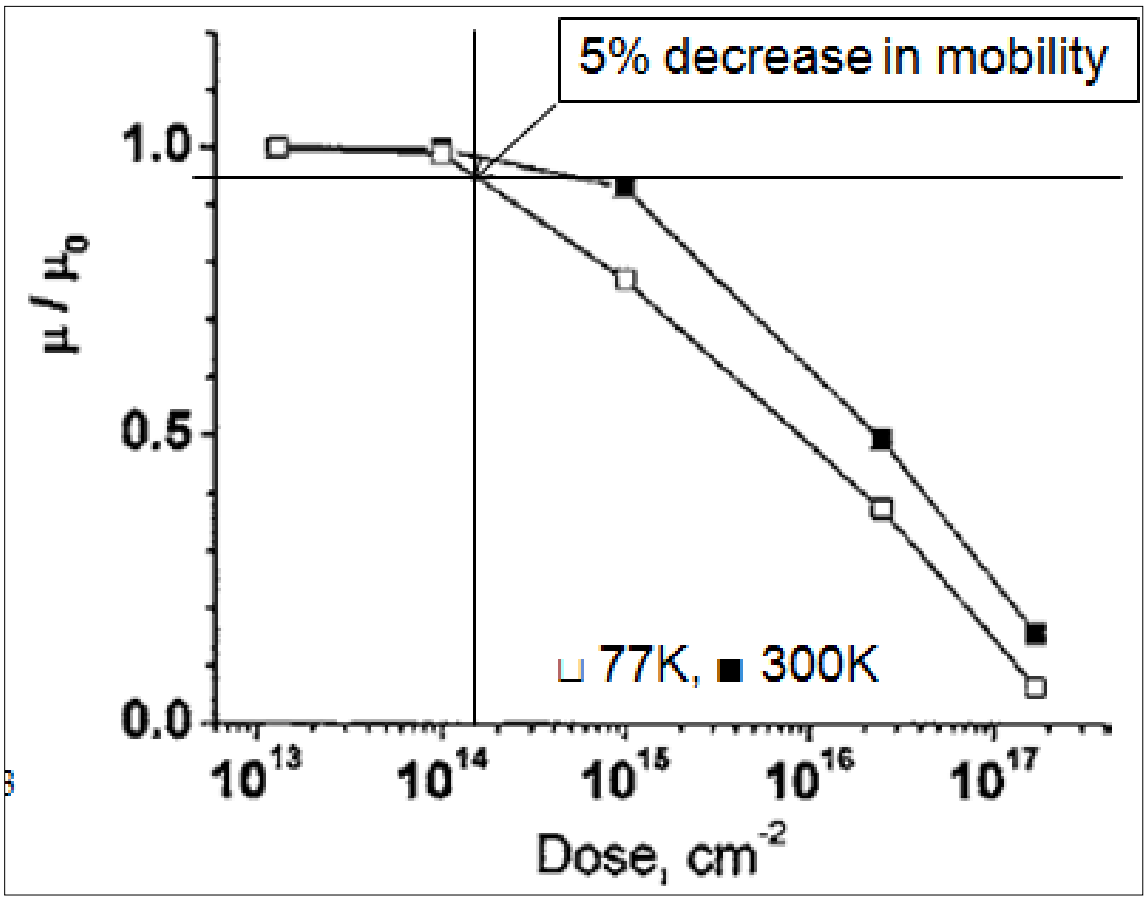

Figure 28. Results of mobility calculations by Polyakov[18]. A 5% decrease in mobility was seen at ~$1.4\text{x}10^{13}$ n/cm^2. Figure reproduced without permission.

The leakage current showed a continuous increase with fluence until $1.25\text{x}10^{13}$ neutrons/cm^2 in both unpassivated, unbiased and biased devices. In order for electrons to

form a leakage current they have to overcome two barriers inside the HFETs structure, first the Schottky barrier at the interface of the metal and AlGaN and a second barrier at the AlGaN/GaN interface. Both, the Schottky and the interface barrier are prone to tunneling if traps lay within the barriers deep below the conduction band. The increase in leakage current observed was attributed to the increase in the trap-assisted tunneling (TAT) caused by trap formation inside the AlGaN layer. Previously it has been suggested that the leakage current is a result of the TAT and direct tunneling. Below 500 K, TAT is the main process responsible for increased leakage current [10]. McClory [15] observed no significant increase in leakage current up to 10^{13} neutrons/cm^2. The Si equivalent 10^{13} n/cm^2 in McClory's study corresponds to $1.25x10^{13}$ GaAs equivalent n/cm^2 used in this research. McClory attributed the limited increase in leakage current due to limited amount oxygen impurities inside the AlGaN layer. The devices used in this study were produced in the same way as the ones used in McClory's research but there was one difference, age. The HFETs used for this research were stored in open air for a long time. It is very likely that the exposed AlGaN layer in unpassivated devices oxidized resulting in more impurities and increasing the possibility of the creation of oxygen complexes initiated by neutron radiation near the surface. This could explain the continuous leakage current increase recorded in Figure 23 and Figure 24. Proposed paths in unpassivated devices responsible for leakage current are shown in Figure 29.

In passivated devices, due to the SiN layer covering the AlGaN the oxidation is expected to be much lower, if not nonexistent. Data presented in Figure 24 supports this

speculation. The change in leakage current is very low, until the fluence of $1.25x10^{13}$ n/cm^2 is reached at which a large increase in I_{gs} was observed.

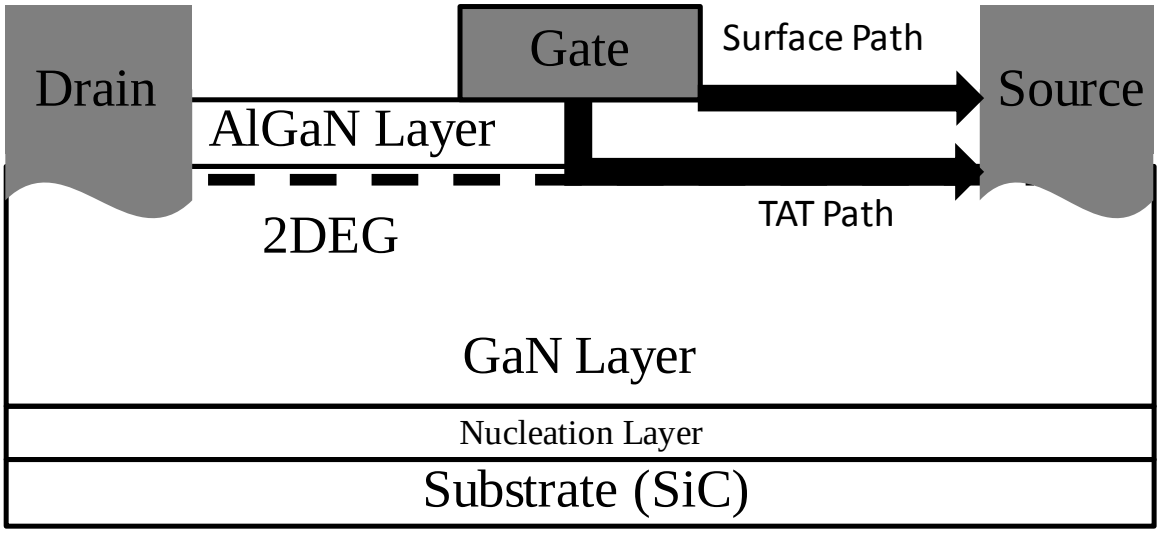

Figure 29. Proposed leakage current paths. The probability of carriers flowing through the path along the top of the AlGaN layer was increased due to irradiation induced oxygen complexing of the AlGaN layer.

No apparent effects of gate biasing during irradiation on HFETs electrical properties were observed in this study. When electron-hole pairs are produced they may separate or recombine. Separation can happen due to the difference between mobilities of holes and electrons [4]. The polarization field inside the HFETs can increase the probability of separation. This field points towards the substrate in the configuration presented in Figure 1. When the gate is biased, the field across the AlGaN layer is reduced.

Originally, it was hypothesized that negatively biasing the gate would change the recombination rate by counteracting the polarization induced field. It is possible that the net changes in the field due to the applied gate bias did not affect the recombination rate of electron-hole pairs significantly. Another explanation for this lack of change could be

the fact that the gate bias was turned off for the duration of measurements, causing the carriers to be swept away.

Only two HFETs survived the neutron irradiation and anneal period. The two possible mechanisms responsible for complete failure of HFETs are: 1) the destruction of the 2 DEG layer via damage to the lattice such that the 2 DEG effectively shuts down and/or 2) carrier mobility degradation, both discussed earlier. This 2 DEG damage is not very likely as research has shown that the changes in the sheet charge density are not significant until fluences of 10^{15} neutrons/cm^2 and above are achieved [17][18]. The more likely process responsible for device failure then is the carrier mobility degradation, at least in the case of device U10. The data shown in Figure 30 supports this assumption.

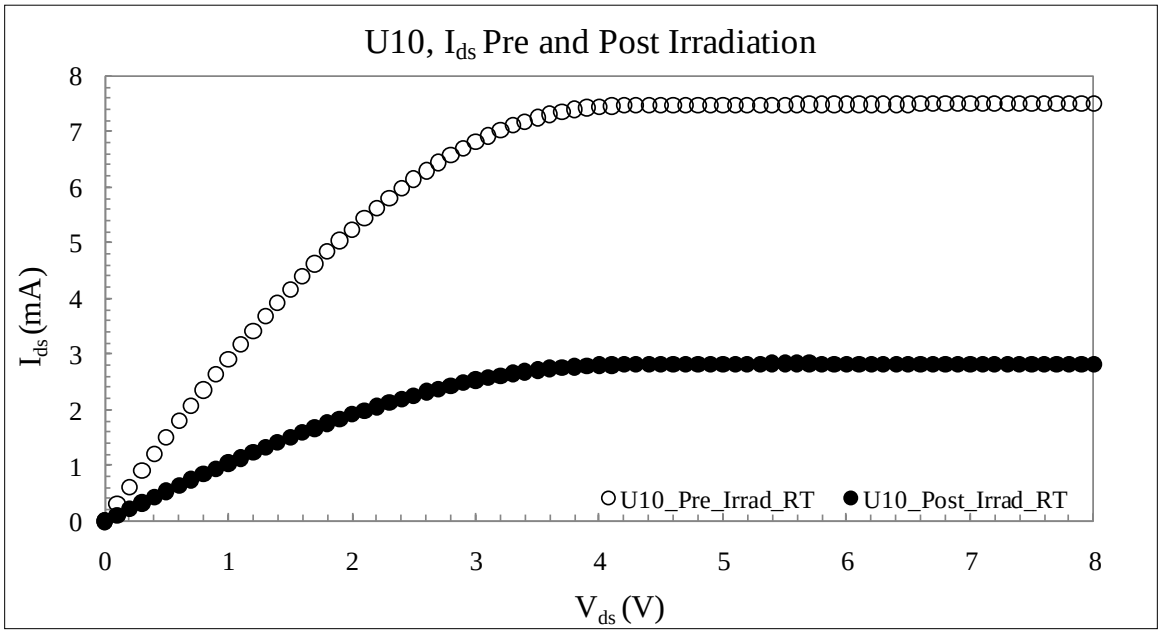

Figure 30. RT Transistor current reduction, pre and post irradiation. A 62% reduction in I_{ds} was attributed to reduction in carrier mobility due to mobile charge defects.

A drastic reduction of over 62% in I_{ds} was seen after the device was brought to 300 K after neutron irradiation, but the device still maintained transistor-like behavior. These HFETs were exposed to ambient during storage. This could have resulted in damage to interfaces and through the AlGaN layer due to oxidation. Additional damage could have been created by electrostatic discharge after removal of HFETs from the testing apparatus. All experiments were conducted during winter months when the relative air humidity is low, increasing the possibility of static discharge.

VI. Conclusions and Recommendations

AlGaN/GaN HFETs have subjected to neutron irradiation up to 7.4×10^{13} 1 MeV GaAs equivalent neutrons/cm^2 with and without biasing the gate. Neutron irradiation caused a variety of defects and charges inside the AlGaN which affected the electrical performance of the HFETs. The method for evaluating transistors performance was the assessment of changes in transistor current, threshold voltage shift, gate leakage current and gate capacitance. The summary of the effects on HFETs is presented here.

1. Transistor Current (I_{ds}) Changes

All unpassivated devices showed an increase (maximum 16.7%) in current relative to pre-irradiation values until a critical fluence (1.25×10^{13} neutrons/cm^2) was achieved. After reaching this fluence, transistors showed continuous degradation in I_{ds} until failure resulted even after removal of devices from the radiation environment.

Passivated, unbiased device showed smaller increase in I_{ds} (~4%) than the unpassivated devices, whereas the passivated, biased HFET showed virtually no change in I_{ds} until the critical fluence was reached.

The increase in I_{ds} was attributed to an increase in the positive charge concentration inside the AlGaN layer. These positive charges are immobile at 120 K and increase the magnitude of the polarization field, effectively increasing the 2 DEG concentration. The decrease in the I_{ds} at higher fluences was a result of mobility degradation due to scattering from defects near the 2 DEG.

2. Threshold Voltage (V_{th}) Shifts

Threshold voltage shifts were observed in all unpassivated and passivated devices. These changes were related to reactor power changes, showing an increase (more negative) every time the power was stepped up. Passivated devices exhibited relatively lower shifts than the unpassivated devices. Calculated sheet concentrations and carrier mobility supports the Rashmi model and is consistent with McClory et al., [15][16] [17][18][19]. On average the threshold voltage changes in unpassivated device shifted by a maximum of 9%. The passivated unbiased device had a maximum shift of ~4% and the biased one ~1%.

3. Leakage Current ($I_{leakage}$) Changes

The leakage current increased steadily with fluence in all unpassivated devices and peaked at ~18 percent. Unlike a similar previous study [15] where no additional increase in the leakage current was observed after 10^{10} n/cm^2, in this study the change was gradual and seemed to peak around $1.25x10^{13}$ n/cm^2. A much smaller change was observed in passivated devices, both biased and unbiased. This seems to support previous claims [15][16][27][28] that passivation minimizes radiation effects. No conclusions have been made to the mechanism behind the differences in leakage current between the unbiased and biased passivated samples, more data needs to be collected in order to investigate the differences.

The observed leakage current overall increase in unpassivated devices was attributed to the creation of traps inside the AlGaN layer and oxygen complexes near the surface of

the AlGaN layer. The interface traps effectively lowered the interface barrier resulting in TAT current increase [10].

4. Recommendations for Future Research

With the newly acquired semiconductor characterization system a new window opened up to improve the accuracy of measurements. The easy setup and speed of data acquisition makes it possible to take data quickly and effortlessly when compared to older systems. An enormous amount of data can be created in a relatively short period of time, providing extra time to test many more devices and therefore improving accuracy.

The change in interface trap concentration during irradiation could be determined using the conductance method [32]. Applying the conductance method would require the acquisition of well- behaved C-V curves. As observed in this research program, well-behaved, in-situ C-V curves are difficult to acquire. Electromagnetic interference and long cables negatively affect the ability to acquire these C-V curves. Better shielded may help to mitigate these effects however maximizing cable shielding can increase neutron activation due to an increase in the total mass of equipment inside the reactor. If C-V measurements are the focus of a future research effort, I recommend that they be the primary measurement technique due to these challenges. I believe that a very well designed experiment can achieve the goal of collecting C-V curves that would allow the determination of changes to interface trap concentration.

The author did not have a chance to investigate the Schottky contact degradation under radiation as planned. The facilities to wire the C-V rings (Figure 10) were under renovation and additional device production was also shut down. Studying the C-V rings

alone would help separate the Schottky contact response to neutron, gamma or electron radiation from the total response of HFETs.

Another possibility for further investigation is continuing the measurement well after the neutron radiation has stopped. Taking a variety of I-V (leakage current, conductance, I_{ds}) and C-V measurements could provide insight in to the failure mechanism of HFETs under high fluences and afterwards. This should be easily accomplished provided constant liquid nitrogen cooling as the semiconductor characterization system can acquire data with little or no input once it's properly setup.

Appendix A

1. OSURR Spectrum Analysis

Equivalent Monoenergetic Neutron Fluence

```
Emin : 1.03 10^-10 | MeV | ;
Emax : 18 | MeV | ;

SetDirectory[ "F:\\AFIT\\Thesis Stuff"] ;

DamageGaAs : Import[ "Damage_GaAs.csv"] ;
FDGaAs : Interpolation[ DamageGaAs] ;

LogLogPlot[ FDGaAs[ x] , { x, 1 10^-10, 20} , PlotStyle → { Black}]
```

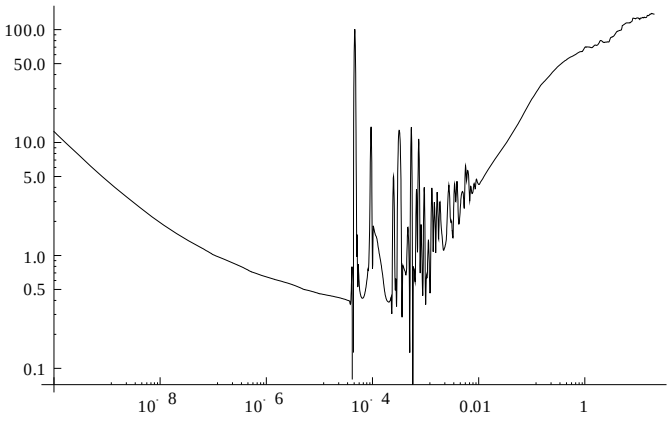


```
DamageSi : Import[ "Damage_Si.csv"] ;
FDSi : Interpolation[ DamageSi] ;

LogLogPlot[ FDSi[ x] , { x, 1 10^-10, 20} , PlotStyle → { Black}]
```

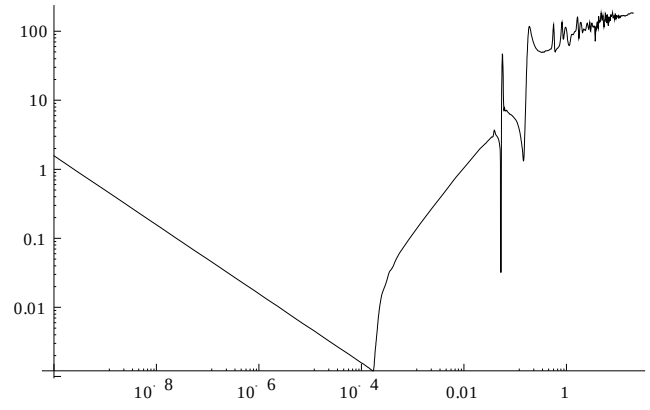

```
Spectrum = Import["Spectrum.csv"];
f = Interpolation[Spectrum];

LogLogPlot[f[x], {x, Emin, Emax}, PlotStyle → {Black}]
```

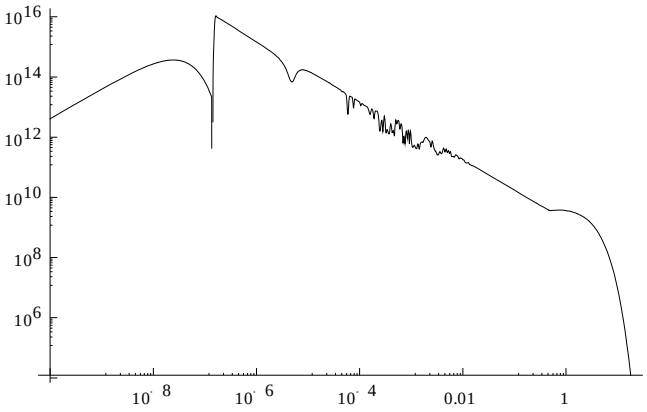

Comparison of Flux with and removed singularities in interpolating function

```
NIntegrate[f[x], {x, Emin, 1.35 * 10^-7}, MaxRecursion → 12] +
 NIntegrate[f[x], {x, 1.4 * 10^-7, 4.9 * 10^-6}, MaxRecursion → 40] +
 NIntegrate[f[x], {x, 4.91 * 10^-6, 5.92 * 10^-5}, MaxRecursion → 40] +
 NIntegrate[f[x], {x, 5.94 * 10^-5, 0.000076}, MaxRecursion → 40] +
 NIntegrate[f[x], {x, 0.0000761, .00016}, MaxRecursion → 40] +
 NIntegrate[f[x], {x, .0001601, .01}, MaxRecursion → 40] +
 NIntegrate[f[x], {x, .01, .5}, MaxRecursion → 40] +
 NIntegrate[f[x], {x, .51, 20}, MaxRecursion → 40]
```

3.04406×10^{10}

```
NIntegrate[f[x], {x, Emin, Emax}, MaxRecursion → 40]
```

3.04797×10^{10}

```
eqGaAs[E_] := NIntegrate[f[x] FDGaAs[x], {x, Emin, Emax}, MaxRecursion → 40] / FDGaAs[E];

eqGaAs[1] * " equivalent neutrons/cm^2 Equivalent Flux at Energy (E) at 100 kW";
```

1.27536×10^{10}

```
eqSi[E_] := NIntegrate[f[x] FDSi[x], {x, Emin, Emax}, MaxRecursion → 15] / FDSi[E];

eqSi[1] * " equivalent neutrons/cm^2 Equivalent Flux at Energy (E) at 100 kW";
```

1.05039×10^{10}

2. Data Acquisition System Settings

Keithley Instruments - Model 4200 system configuration information

System Information:

Model: Keithley Model 4200-SCS Semiconductor Characterization System	
Date	11/21/2009 Eastern Standard Time
System name	4200SCS-1139695
System serial number	1139695
Platform version	4200-300-2Q
Operating system version	4200-852-5.0
KTE Interactive version	V7.1
Powerline frequency	60 HZ
KXCI Settings	SMU1 = SMU1
	SMU2 = SMU2
	SMU3 = SMU3
	SMU4 = NONE
	SMU5 = NONE
	SMU6 = NONE
	SMU7 = NONE
	SMU8 = NONE
	GPIB Address = 17
	Delimiter = COMMA
	EOI = ON
	4145 Emulation = OFF

	Communication = GPIB
	PortNumber = 1225
User Library Directory	C:\S4200\kiuser\usrlib

Instrumentation:

Model: Keithley Instruments 4200-SMU Medium Power Source Measure Unit	
Instrument ID	SMU1
Slot number	1
Firmware version	H21
Hardware version	5.3C:493198
Serial number	1213506
Calibrated on date	Oct 23, 2008
Calibration due on	Oct 23, 2009
Model: Keithley Instruments 4200-SMU Medium Power Source Measure Unit	
Instrument ID	SMU2
Slot number	2
Firmware version	H21
Hardware version	5.3C:493198
Serial number	1213535
Calibrated on date	Oct 23, 2008
Calibration due on	Oct 23, 2009
Model: Keithley Instruments 4200-SMU Medium Power Source Measure Unit	
Instrument ID	SMU3
Slot number	3
Firmware version	H21
Hardware version	5.3C:493198
Serial number	1213537

Calibrated on date	Oct 23, 2008
Calibration due on	Oct 23, 2009
Model: Keithley Instruments 4200-CVU Multi-Frequency Capacitance Voltage Measure Unit	
Instrument ID	CVU1
Slot number	4
Firmware version	1.03
Hardware version	3.0:489248
Serial number	Z004522
Calibrated on date	Oct 23, 2008
Calibration due on	Oct 23, 2009
Model: Keithley Instruments 4200-SCOPE	
Instrument ID	OSC1
Slot number	7
Firmware version	1.34
Hardware version	
Serial number	21245
Channel 1 ID	INPUT 1
Channel 2 ID	INPUT 2
Model: Keithley Instruments 4205-VPU Voltage Pulse Unit	
Instrument ID	VPU1
Slot number	8
Firmware version	1.01
Hardware version	1.11:490179
Serial number	Z005158
Channel 1 ID	OUTPUT 1
Channel 2 ID	OUTPUT 2
Calibrated on date	Oct 23, 2008
Calibration due on	Oct 23, 2009
Channel 1 - High	Enabled

Channel 2 - High	Enabled
Model: Keithley Instruments 4200 Ground Unit	
Instrument ID	GNDU
Model: Generic Test Fixture	
Instrument ID	TF1
Number of pins	12
Model: General Purpose 2-Wire Test Instrument	
Instrument ID	GPI1
GPIB Address	1
Model: Keithley Instruments 707/707A Switching Matrix	
Instrument ID	MTRX1
GPIB Address	18
Connection scheme	Row-Column
Sense scheme	Local Sense
Slot 1	Keithley 7174 Low Current Matrix Card
Slot 2	Empty
Slot 3	Empty
Slot 4	Empty
Slot 5	Empty
Slot 6	Empty

Connections:

Instrument ID	Terminal Name	Terminal ID	Matrix
SMU1	FORCE	SMU1	ROWA
SMU1	SENSE	-	NC
SMU2	FORCE	SMU2	ROWB
SMU2	SENSE	-	NC

SMU3	FORCE	SMU3	ROWC
SMU3	SENSE	-	NC
CVU1	CVH_CUR	CVH1	ROWF
CVU1	CVH_POT	-	ROWF
CVU1	CVL_CUR	CVL1	ROWE
CVU1	CVL_POT	-	ROWE
GNDU	FORCE	GNDU	ROWD
GNDU	SENSE	-	NC
GPI1	HI	GPI1	ROWH
GPI1	LO	GPI1L	ROWG
TF1	PIN1 Force	1	COLUMN1
TF1	PIN1 Sense	1	NC
TF1	PIN2 Force	2	COLUMN2
TF1	PIN2 Sense	2	NC
TF1	PIN3 Force	3	COLUMN3
TF1	PIN3 Sense	3	NC
TF1	PIN4 Force	4	COLUMN4
TF1	PIN4 Sense	4	NC
TF1	PIN5 Force	5	COLUMN5
TF1	PIN5 Sense	5	NC
TF1	PIN6 Force	6	COLUMN6
TF1	PIN6 Sense	6	NC
TF1	PIN7 Force	7	COLUMN7
TF1	PIN7 Sense	7	NC

TF1	PIN8 Force	8	COLUMN8
TF1	PIN8 Sense	8	NC
TF1	PIN9 Force	9	COLUMN9
TF1	PIN9 Sense	9	NC
TF1	PIN10 Force	10	COLUMN10
TF1	PIN10 Sense	10	NC
TF1	PIN11 Force	11	COLUMN11
TF1	PIN11 Sense	11	NC
TF1	PIN12 Force	12	COLUMN12
TF1	PIN12 Sense	12	NC

Bibliography

[1] Hu, X., A. P. Karmarkar, et al. (2003). "Proton-irradiation effects on AlGaN/ AlN/ GaN high electron mobility transistors," *Transactions on Nuclear Science, IEEE* 50(6): 1791-1796.

[2] Ionascut-Nedelcescu, A., C. Carlone, et al. (2002). "Radiation hardness of gallium nitride," *Transactions on Nuclear Science, IEEE* 49(6): 2733-2738.

[3] H.Markoc, "Nitride Semi-conductors and Devices," Springer-Verlag Berlin Heidelberg, 1999.

[4] Yen-Kuang Kuo, et al., "Band-Gap Bowing Parameter of the $Al_xGa_{1-x}N$ Derived from Theoretical Simulation," *The Japan Society of Applied Physics*, Vol. 41 (2002) pp. 73–74 Part 1, No. 1, January 2002

[5] O. Ambacher, R. Dimitrov, W. Rieger, et al., "Two-dimensional electron gases induced by spontaneous and piezoelectric polarization charges in N- and Ga-face AlGaN/GaN heterostructures," *Journal of Applied Physics*, vol. 85, no. 6, pp. 3222-3333 1999.

[6] A. Rashmi, Kranti, et al., "An accurate charge control model for spontaneous and piezoelectric polarization dependent two-dimensional electron gas (2-DEG) sheet charge density of lattice mismatched AlGaN/GaN HEMTs," *Solid-State Electronics*, 46(5): 621-630, 2002.

[7] A.F.M. Anwar, et al., "Schottky barrier height in GaN/AlGaN heterostructures," *Solid State Electronics*, 19 April 2006.

[8] S.M Sze, K.NG Kwok, "*Physics of Semiconductor Devices*," John Wiley & Sons, Inc. Publication, 2007

[9] L. Hsu, W. Walukiewicz, "Electron mobility in $Al_xGa_{1-x}N$/GaN heterostructures," *Physical Review B*, vol. 56, no. 3, pp. 1520, 1997.

[10] D. K. Schroder, "*Semiconductor Material and Device Characterization*," 3nd Edition, John Wiley & Sons, New York, 2006.

[11] S. Karmalkara et al., "Mechanism of the reverse gate leakage in AlGaN/GaN high electron mobility transistors," *Applied Physics Letters*, vol.82, no. 22, 2 June 2008.

[12] D. M. Sathaiya, et al., "Thermionic trap-assisted tunneling model and its application to leakage current in nitrided oxides and AlGaN/GaN high electron mobility transistors," *Journal of Applied Physics*, 11 May 2006.

[13] C. Svensson, I. Lundstrom, "Trap assisted charge injection in MNOS structures," *Journal of Applied Physics*, vol. 44, no. 10, pp. 4657, 1973.

[14] M.R Hogsed, "*Deep Level Defects in Electron-Irradiated Aluminum Gallium Nitride Grown by Molecular Beam Epitaxy*," Air Force Institute of Technology (AU), Wright-Patterson AFB, OH, 2005

[15] J.W McClory, "*The Effects of Radiation on the Electrical Properties of Aluminum Gallium Nitride Gallium Nitride Heterostructures*," Air Force Institute of Technology (AU), Wright-Patterson AFB, OH, 2008

[16] J.T Moran, "*The Effect of Temperature and Electron Radiation on the Electrical Properties of AlGaN/GaN Heterostructure Field Effect Transistors*," Air Force Institute of Technology (AU), Wright-Patterson AFB OH, 2009

[17] M.L. Zhang, et al., "Neutron Irradiation Effect in Two-Dimensional Electron Gas of AlGaN/GaN Heterostructures," *Chinese Physics Letters*, vol. 25, no. 3, 1045, 2008.

[18] A. Y. Polyakov, et al., "Neutron irradiation effects on electrical properties and deep-level spectra in undoped n-AlGaN/GaN heterostructures," *Journal of Applied Physics*, vol. 98, 033529, 2005.

[19] A. Y. Polyakov, et al., "Neutron irradiation effects in AlGaN/GaN heterojunctions," *Physica B* 376–377, 523–526, 2006

[20] P. Kordos, P. Kudela, D. Gregusova, D. Donoval, "The effect of passivation on the performance of AlGaN/GaN heterostructure field effect transistors," *Semiconductor Science and Technology*, vol. 21, no. 12, pp. 1592-1596, December 2006.

[21] W.P. Gu, et al., "High-electric-field-stress-induced degradation of SiN passivated AlGaN/GaN high electron mobility transistors," *Chinese Phys. B* 18 1601-1608, 2009

[22] B.D. White, et al., "Characterization of 1.8-MeV Proton-Irradiated AlGaN/GaN Field-Effect Transistor Structures by Nanoscale Depth-Resolved Luminescence Spectroscopy," *IEEE Transactions on Nuclear Science*, Vol. 49, No. 6, pp. 2695-2701, December 2002

[23] F. Gaudreau, et al., "Transport Properties of Proton-Irradiated Gallium Nitride-Based Two-Dimensional Electron-Gas System," *IEEE Transactions on Nuclear Science*, Vol. 49, No. 6, pp. 2702-2707, December 2002

[24] X.Hu, et al., "The Energy Dependence of Proton-Induced Degradation in AlGaN/GaN High Electron Mobility Transistors," *IEEE Transactions on Nuclear Science*, Vol. 51, No. 2, December 2004

[25] T.A Uhlman, "*Temperature Dependent Current-Voltage Measurements of Neutron Irradiated $Al_{0.27}Ga_{0.73}N/GaN$ Modulation Doped Field Effect Transistors*," Air Force Institute of Technology (AU), Wright-Patterson AFB, OH, 2005

[26] T. E. Gray, "*Investigation of Gate Current in Neutron Irradiated AlGaN/GaN Heterostructure Field Effect Transistors Using Voltage and Temperature Dependence*," Air Force Institute of Technology (AU), Wright-Patterson AFB, OH, March 2007.

[27] O. Aktas, et al., "^{60}Co gamma radiation effects on DC, RF, and pulsed I-V characteristics of AlGaN/GaN HEMTs," *Solid State Electronics*, vol. 48, pp. 471-475, 2004.

[28] B. Luo , et al., "Influence of ^{60}Co gamma-rays on dc performance of AlGaN/GaN high electron mobility transistors," *Applied Physics Letter*, vol. 80, Number 4 28 January 2002

[29] J. Talnagi, Personal Communications, January 2010.

[30] X. Hu, et al., "Proton-irradiation effects on AlGaN/AlN/GaN high electron mobility transistors," *IEEE Transactions on Nuclear Science*, vol. 50, no. 6, pp. 1791-1796, Dec. 2003.

[31] Y. Zhang, I. P. Smorchkova, C. R. Elsass, S. Keller, J. P. Ibbetson, S.DenBaars, U. K. Mishra, and J. Singh, "Charge control and mobility in AlGaN/GaN transistors: Experimental and theoretical studies," *Journal of Applied Physics*, vol. 87, no. 11, pp. 7981–7987, 2000.

[32] T. Aggerstam, S. Lourdudoss, H.H. Radamson, M. Sjödin, P. Lorenzini and D.C. Look, "Investigation of the interface properties of MOVPE grown AlGaN/GaN high electron mobility transistor (HEMT) structures on sapphire," *Proceedings of the Eighth International Conference on Atomically Controlled Surfaces, Interfaces and Nanostructures and the Thirteenth International Congress on Thin Films*, Volume 515, Issue 2, Pages 705-705, October 2006.

[33] E.H Nicollian, A.Goetzberger, "The Si-SiO2 Interface-Electrical Properties as Determined by the Metal-Insulator-Silicon Conductance Technique," *Bell Syst. Tech. J.* 46, 1055-1133, July/August. 1967

REPORT DOCUMENTATION PAGE

Form Approved
OMB No. 0704-0188

1. REPORT DATE *(DD-MM-YYYY)*	**2. REPORT TYPE**	**3. DATES COVERED** *(From - To)*
27-03-2010	Master's Thesis	Sep 2008 – Mar 2010

4. TITLE AND SUBTITLE

In-situ, Gate Bias Dependent Dtudy of Neutron Irradiation Effects on AlGaN/GaN HFETs

5a. CONTRACT NUMBER

5b. GRANT NUMBER

5c. PROGRAM ELEMENT NUMBER

6. AUTHOR(S)

Mikina, Janusz K., Captain, USAF

5d. PROJECT NUMBER
N/A

5e. TASK NUMBER

5f. WORK UNIT NUMBER

7. PERFORMING ORGANIZATION NAME(S) AND ADDRESS(ES)

Air Force Institute of Technology
Graduate School of Engineering and Management (AFIT/EN)
2950 Hobson Way
WPAFB OH 45433-7765

8. PERFORMING ORGANIZATION REPORT NUMBER

AFIT/GNE/ENP/10M-06

9. SPONSORING / MONITORING AGENCY NAME(S) AND ADDRESS(ES)

Defense Threat Reduction Agency
COL Mark Mattox
1900 Wyoming Blvd SE
Kirtland AFB, NM 87117-5669

10. SPONSOR/MONITOR'S ACRONYM(S)

DTRA/CSU

11. SPONSOR/MONITOR'S REPORT NUMBER(S)

12. DISTRIBUTION / AVAILABILITY STATEMENT

APPROVED FOR PUBLIC RELEASE; DISTRIBUTION UNLIMITED

13. SUPPLEMENTARY NOTES

14. ABSTRACT

In this study, unpassivated and SiN passivated $Al_{0.27}Ga_{0.73}N$/GaN HFETs were subjected to neutron radiation at 120 K. The primary focus of the research was the effects of neutron irradiation on drain current, gate leakage current, threshold voltage shift, gate-channel capacitance, and the effects of biasing the gate during irradiation. In-situ measurements were conducted on transistor current, gate-channel capacitance, and gate leakage current vs. gate bias beginning at 77 K through 300 K in 4 K temperature intervals. The drain currents increased for all devices, with a lesser increase observed for passivated devices. The changes in carrier concentration and carrier mobility, obtained from observed drain current increases and calculated with the charge control model using observed threshold voltage shifts, were attributed to trapped, positive charges in the AlGaN layer. This trapped positive charge resulted from electron-hole pairs created by neutron radiation-induced ionizations. The leakage current increased in all devices, with a smaller change observed in passivated devices. This increase was attributed to the formation of interface traps. Biasing the gate under neutron irradiation had no effect on electrical performance of HFETs.

15. SUBJECT TERMS
AlGaN, GaN, Aluminum Gallium Nitride, HFET, 2DEG, Trap-Assisted Tunneling, TAT, Heterostructure Field Effect Transistors, Mobility, In-Situ

16. SECURITY CLASSIFICATION OF: UNCLASSIFIED			**17. LIMITATION OF ABSTRACT**	**18. NUMBER OF PAGES**	**19a. NAME OF RESPONSIBLE PERSON**
a. REPORT	**b. ABSTRACT**	**c. THIS PAGE**			John W. McClory (ENP)
U	U	U	UU	88	**19b. TELEPHONE NUMBER** *(include area code)* (937) 255-3636, ext 7308

Standard Form 298 (Rev. 8-98)
Prescribed by ANSI Std. Z39.18